

**Best
Available
Copy**

AD-756 681

Investigation of the Feasibility of the Electron Beam-Excited, High-Pressure Recombination Laser

Texas University

**prepared for
Office of Naval Research**

FEBRUARY 1973

Distributed By:

NTIS

**National Technical Information Service
U. S. DEPARTMENT OF COMMERCE**

N00014-67-A-0310-0007

UTOP A003-1

AD756681

RECOMBINATION LASER

Annual Report

by

C. B. COLLINS

A. J. CUNNINGHAM

W. B. JOHNSON

DDC
RECEIVED
MAR 12 1973
REGULATED
B

Reproduced by
NATIONAL TECHNICAL
INFORMATION SERVICE
U.S. Department of Commerce
Springfield, VA 22151

DISTRIBUTION STATEMENT A

Approved for public release;
Distribution Unlimited

prepared for
OFFICE OF NAVAL RESEARCH
DEPARTMENT OF THE NAVY
sponsored by
ADVANCED RESEARCH PROJECTS AGENCY
FEBRUARY 1973

R
119

Security Classification

DOCUMENT CONTROL DATA - R & D

(Security classification of title, body of abstract and indexing annotation must be entered when the overall report is classified)

1. ORIGINATING ACTIVITY (Corporate author) The University of Texas at Dallas P. O. Box 30365 Dallas, Texas 75230		2a. REPORT SECURITY CLASSIFICATION UNCLASSIFIED	
		2b. GROUP	
3. REPORT TITLE INVESTIGATION OF THE FEASIBILITY OF THE ELECTRON BEAM-EXCITED, HIGH-PRESSURE RECOMBINATION LASER			
4. DESCRIPTIVE NOTES (Type of report and inclusive dates) First Annual Technical Report (period covered by this report 3/21/72-12/31/72)			
5. AUTHOR(S) (First name, middle initial, last name) Carl B. Collins Austin J. Cunningham Brian W. Johnson			
6. REPORT DATE 28 February 1973		7a. TOTAL NO. OF PAGES 116	7b. NO. OF REFS 16
8a. CONTRACT OR GRANT NO. N00014-67-A-0310-0007		9a. ORIGINATOR'S REPORT NUMBER(S) UTDP A003-1	
b. PROJECT NO. ARPA Order No. 1807			
c. Program Code 2E90		9b. OTHER REPORT NO(S) (Any other numbers that may be assigned this report)	
d.			
10. DISTRIBUTION STATEMENT Distribution of this document is unlimited.			
11. SUPPLEMENTARY NOTES		12. SPONSORING MILITARY ACTIVITY Office of Naval Research	
13. ABSTRACT This report describes research applied toward the determination of the feasibility of developing a recombining, electron beam-excited plasma into a pulsed laser of exceptionally high peak power.			

DD FORM 1473
1 NOV 65

UNCLASSIFIED

Security Classification

Security Classification

14.

KEY WORDS

LINK A

LINK B

LINK C

ROLE

WT

ROLE

WT

ROLE

WT

Recombination Laser

Laser

FIRST ANNUAL TECHNICAL REPORT

Item A003

Short Title: RECOMBINATION LASER

ARPA Order Number 1807

Program Code Number 2E90

Contract Number N00014-67-A-0310-0007

Principal Investigator: C. B. Collins
The University of Texas at Dallas
P. O. Box 30365
Dallas, Texas 75230
(214) 231-1471

Contractor: The University of Texas at Dallas

Scientific Officer: Director
Physics Programs,
Physical Sciences Division,
Office of Naval Research
Department of the Navy
800 N. Quincy Street
Arlington, Virginia 22217

Effective Date of Contract: 21 March 1972

Expiration Date of Contract: 31 December 1973

Period Covered by this Report: 21 March 1972 - 31 December 1972

Amount of Basic Contract: \$ 99,990

Amount of Modification #1: 91,400

Total Contract: \$191,390

Sponsored by

Advanced Research Projects Agency

ARPA Order No. 1807

Form Approved Budget Bureau No. 22-RO293

The views and conclusions contained in this document are those of the authors and should not be interpreted as necessarily representing the official policies, either expressed or implied, of the Advanced Research Projects Agency of the U.S. Government.

CONTENTS

Item	Page
I. TECHNICAL REPORT SUMMARY	1
II. INTRODUCTION AND BACKGROUND.	6
III. EXPERIMENTAL METHOD.	17
IV. TECHNICAL RESULTS.	41
V. IMPLICATIONS.	107

I. TECHNICAL REPORT SUMMARY

The objective of the research described in this report is to determine the feasibility of developing a recombining electron beam-excited plasma into a pulsed laser of exceptionally high peak power. Currently accepted theory indicates that this should be possible.

Although a wide variety of recombination processes are known to occur in gaseous plasmas, it is only the relatively complex and unfamiliar collisionally-stabilized one which appears to hold promise for a lasing medium. As discussed in Section II, this process is optimized at high charge densities and relatively low energies, but is almost completely quenched in atomic and molecular systems which can participate in dissociative recombination. Theory predicts that in helium at charge densities of the order of 10^{16} cm^{-3} collisionally-stabilized recombination should produce large inverted population of the resulting neutrals which would tend to radiate in the 2.0μ to 0.3μ wavelength region, provided the temperature of the electron swarm is kept low. It is this requirement which suggests that unlike conventional visible and UV lasers excited by electron beams, lasing action from recombination would be optimized in the afterglow period following the termination of the beam. There is a considerable advantage in this from the viewpoint of fundamental collision cross-sections. In the conventional, directly-excited visible and UV systems over 95% of the beam energy is lost to the production of ionization not contributing to the laser output. In contrast and as detailed in Section II, theory has predicted that the subsequent collisionally-stabilized recombination of the ions with electrons could provide a mechanism for recovering some of this ionization energy with a resulting orders of magnitude increase in the optical output.

Both the available output energy and pulse duration depend strongly on the electron density, high values of which only become available from e-beam excitation at high neutral gas pressures. In this requirement lies the basic uncertainty in the approach since previous investigations of this type of charge neutralization have centered on neutral gas densities some 200 times less than the 20 atmosphere values which theory requires for significant radiative output.

The research effort reported here has focused upon this recombination approach and the intent of the initial considerations have been to first provide an additional test of theory in helium at an intermediate pressure of three atmospheres. From it can be directly determined the amount of light output, the lifetime of the recombination process, and whether or not population inversions were developed.

During the current reporting period an electron beam-excited helium afterglow system, operating routinely at 5 atmospheres and capable of modification to 20, was developed and instrumented so that spectroscopic observation of transient emissions in the visible and near IR region could be made with 10 nanosecond resolution. Construction details and system performance are presented in Section III.

Technical results discussed in Section IV appear highly encouraging from the perspective of the contract objective. In particular, it was determined that:

1. In the absence of lasing, incoherent emissions of the order of 0.1 to 1.0 milli-Joules/liter per pulse occurred in the afterglow of the 3 atmospheres of helium at 7065, 6400 and 5875Å. System efficiencies ran as high as 0.04% even without laser action.

2. Both the detailed functional forms and effective lifetimes of the spectral transients were consistent with the theory of collisionally-stabilized recombination as applied to an electron swarm at 1000°K effective temperature. Characteristic lifetimes of the radiating population were found to be about 100 nanoseconds at this pressure for the He_2 bands at 6400Å and 4650Å. The corresponding peak power radiated incoherently at 6400Å was of the order of 1000 watts/liter. Improvements realized in the evolved afterglow cell HPAC-1b sufficiently increased system integrity to allow initial evacuation to better than 10^{-10} Torr with mass spectrometric analysis of the **residual** gas. The resultant increase in gas purity contributed an improvement in energies available from recombination by reducing competing charge transfer channels of de-excitation. At the 7 atmosphere upper limit of pressures, lifetimes were found to decrease to 25 nanoseconds.
3. Optical gain was inferred from measurements of time-resolved enhancement ratios in non-oscillating optical cavities resonant at the wavelengths of the various prominent bands and lines. Positive gain was indicated for all transitions examined not terminating on metastable levels. Gain coefficients of the order of 0.05 per transit of the afterglow were indicated for the helium lines at 6678 and 5875Å. Peak gain coefficients of 0.16 and 0.17 per transit were measured for the atomic line at 7065Å and the molecular band at 6400 Å, respectively. Unfortunately, the shorter wavelength band at 4650Å terminated on a metastable level and showed an absorption coefficient of 0.23 per transit at this pressure.

Implications are that the 6400\AA transition can be lased when the afterglow chamber is fitted with optical-quality Brewster-angle windows. Attempts to verify this indication will be made when the third afterglow chamber containing low-loss windows is installed. Its design will permit operation to 20 atmospheres of helium while maintaining system integrity characteristic of ultra-high vacuum installation. Furthermore, as detailed in Section V, it is indicated that as a consequence of operation at 20 atmospheres lifetimes will decrease to a few nanoseconds with a consequent increase in both pulse energy and peak power. Still to be determined is whether lasing can actually be realized and if so whether the energy currently lost during the recombination to non-radiative channels of stabilization can be returned to an induced radiative channel.

However, should theory continue to be validated, the feasibility of the recombination laser would, in fact, be established. In that case the consequent advantages inherent in the use of the recombination process would be expected to be:

- 1) Visible to near-uv operating wavelengths. The principal molecular Rydberg series in He_2 extends from 6400\AA to 3680\AA .
- 2) One output photon per ion. Most of the excitation energy in inert gases goes into ionization and overall efficiencies of 8% should be attained.
- 3) Lifetimes for the source of population proportional to the inverse cube of the electron density. At 20 atmospheres pressure and an electron density of the order of 10^{16} cm^{-3} , lifetimes of the order of 1.0 nanosecond should be realized.

- 4) Scalable output energies. Of the order of 5 Joules/liter could be expected at electron densities of 10^{16} cm^{-3} . At electron densities of 10^{17} cm^{-3} which are characteristic of 200 atmospheres pressures, 50 Joules/liter would be expected in a picosecond if the same electron temperature were maintained.
- 5) Control of the precise temporal form of the output pulse. This can be controlled in principle by heating the recombining electrons and thus varying the rate of the population supply through its expected $T_e^{-9/2}$ dependence.

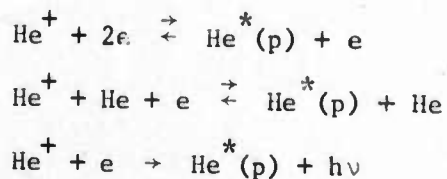
Evidently, the critical point in the course of this research is the immediate future lies in the realization of lasing action in one of the bands. Subsequent optimization would then be dependent upon extensive further research into the detailed steps and thermal economy of the recombination process.

II. INTRODUCTION AND REVIEW

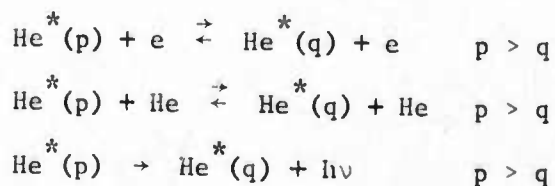
Theory^{1,2,3,4,5} predicts the occurrence of extremely large inversions of populations in certain recombining high pressure plasmas. However, prior to the commencement of the research discussed here, such inversions had only been examined⁶ in low pressure helium afterglows. Indications based on those studies of collisionally-stabilized recombination were that it could in fact form the basis for a new type of laser of high power. In such a device the inversion of population would be produced as a consequence of particular ion-electron recombination processes in which the excited atomic or molecular states are sequentially populated, energetically speaking, from the top down. Although theory had predicted substantial consequent pair inversion ratios for almost a decade⁵, the difficulties in obtaining recombination controlled plasmas of large volume, which at the same time were free from the competing effects of dissociative recombination, generally prevented the actual observation of such inversions.

The process of collisionally stabilized recombination is a complex one occurring, essentially, in two composite steps, 1) capture of an electron by an ion and 2) subsequent stabilization. For example, in helium the sequences are the following:

Capture processes



Stabilization processes



where $\text{He}^*(p)$ denotes an excited helium atom with principal quantum number, p .

The net result of the initial capture sequence is the establishment of a quasi-equilibrium distribution of population among the bound states whose ionization potential is less than a few KT for the electron gas. However, the total population within such states is usually small compared to the ion density and therefore do not represent a significant portion of the loss of ionization due to recombination. Subsequent stabilization can occur by successive collisional or radiative processes which tend to move population to states of greater ionization potential. When an element of population has been moved to a level of sufficiently high ionization potential, the rates for the inverse excitation processes are negligible and the stabilization is complete. It is during the course of this latter sequence of steps that substantial inversions of population should be produced.⁵

Of first importance to the evaluation of collisional radiative recombination as a process for populating inversions in a practical laser medium are its potential in terms of a) output wavelength and pulse energy, b) pulse duration, and c) efficiency. Consideration of each is reviewed in the following subsections:

- a) Output wavelength and pulse energy -- an estimate for these parameters can be made by recognizing that first for a sufficiently high upper state the nearly degenerate sublevels are in thermal equilibrium at the electron temperature and secondly that most collision-induced changes of energy level result in only a unit change in principal quantum level.² In other words, there is no effective mechanism by which the recombining electrons can avoid the upper state of the stimulated transition. Consequently, the least upper boundary on

the number of transitions per pulse which can be stimulated to emit is the number of recombination events occurring in the afterglow period following each ionizing pulse and plasma. Assuming competing losses of ionization can be suppressed, one photon could be obtained for each electron originally produced. Optimization of the energy available would occur by selecting a transition in a Rydberg series of the atom or molecule with principal quantum number as large as possible without elevating the energy into the "quasi-equilibrium group" of levels mentioned above. In principal this means a photon of energy a few KT less than the greatest ionization energy found in the class of states having transitions to states with very short radiative lifetimes. Examples are found in Figures 1 and 2 which shows excited state energies for He and He₂, respectively. In the former the most suitable series would be the $n^3F \rightarrow 3^3D$ commencing at 1.87μ and converging at $\sim 8190 \text{ \AA}$. In the latter species, He₂, the more favorable series, $np^1\Pi_g \rightarrow 2s^1\Sigma_u$, ranging from 5130 \AA to 3130 \AA and $ns^3\Sigma_u^+ \rightarrow 2p^3\Pi_g$ ranging from 6400 \AA to the convergence limit at 3680 \AA could be attempted. In these cases, Table I summarizes the consequent peak pulsed energy available in a recombining helium afterglow of 10^{16} electron-ion pairs/cm³.

Figure 1

Energy level diagram of He. Energies of the excited states have been plotted relative to the ground state which is off-scale to the bottom. Wavelengths of the principal transitions have been indicated.

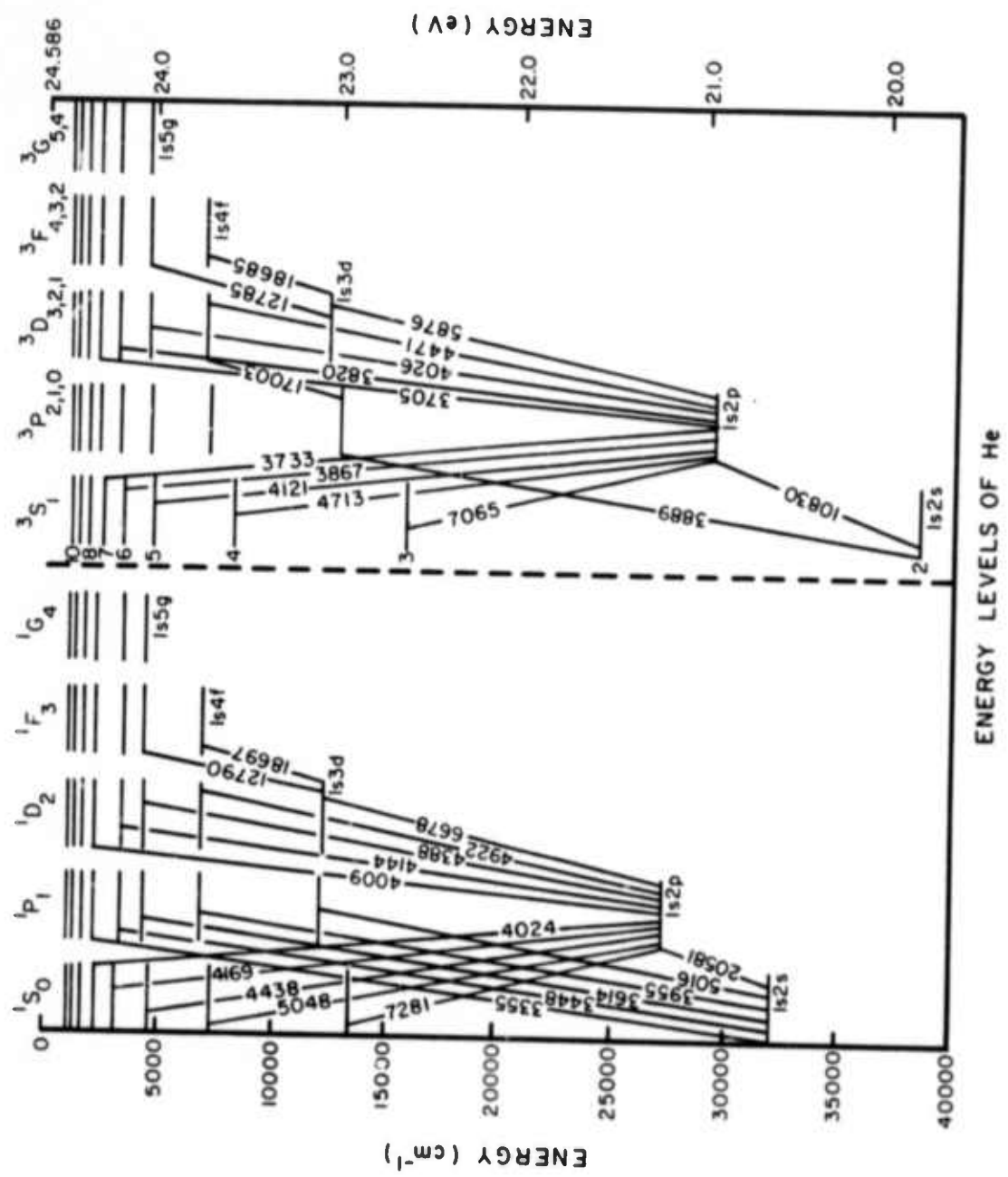


Figure 2

Energy level diagram of He_2 . Values of energy characteristic of the equilibrium internuclear separation have been plotted relative to the lowest metastable $2s^3\Sigma_u^+$ state. The ground state is $1s\sigma^2 2s\sigma^2$ and strongly repulsive at these internuclear separations. Wavelengths of the band origins of principal transitions have been indicated.

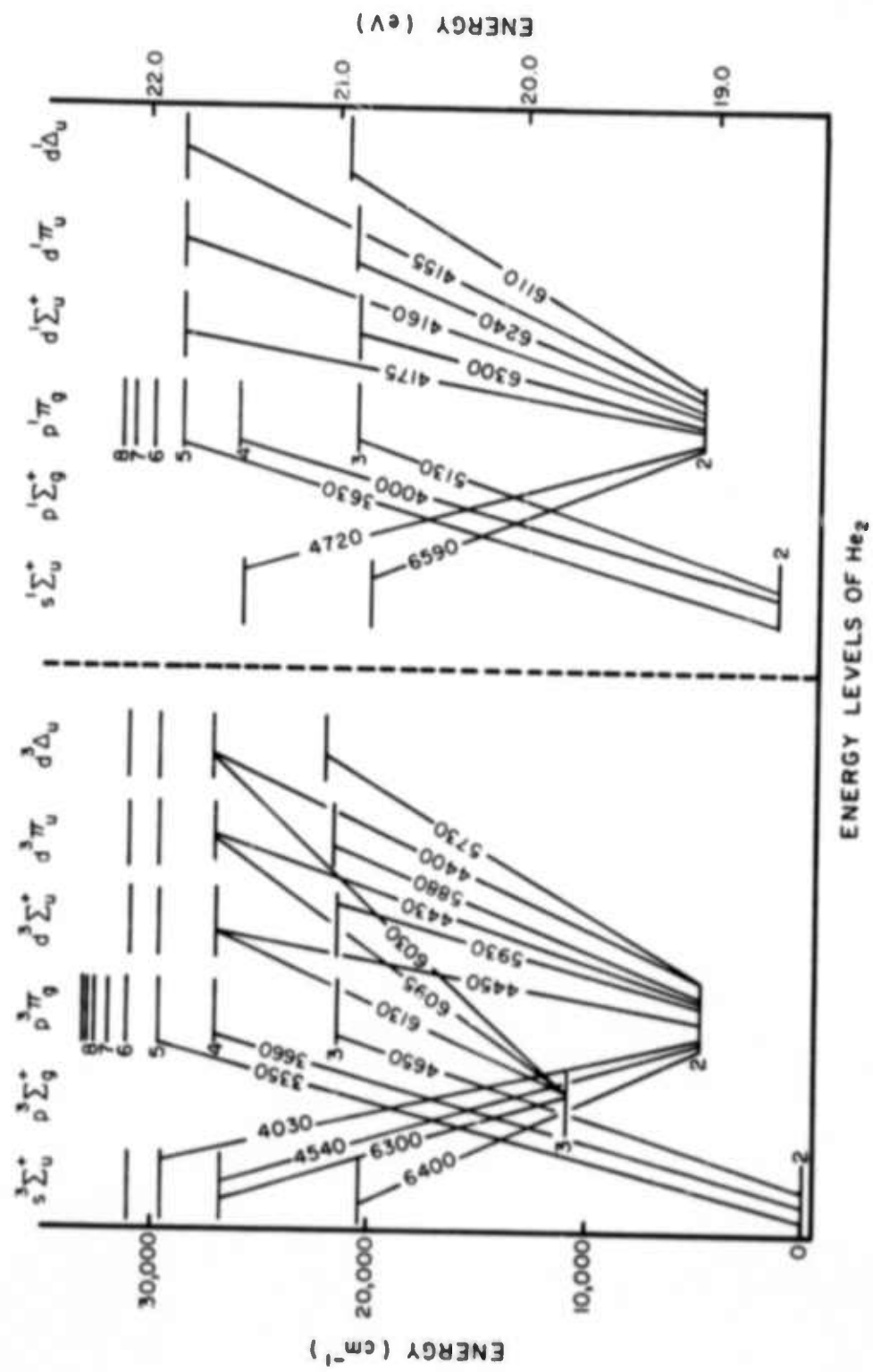


Table I

Peak Pulsed Energies Available in Listed Transitions

Wavelength	Species	State	Quantum Efficiency	Energy (Joule/liter)
18700Å	He	$4^3F \rightarrow 3^3D$	2.7%	1.1
8190Å	He	$11m n^3F \rightarrow 3^3D$	6.2%	2.4
6400Å	He ₂	$3s^3\Sigma_u^+ \rightarrow 2p^3\Pi_g$	8.6%	3.1
5130Å	He ₂	$3p^1\Pi_g \rightarrow 2s^1\Sigma_u$	10.8%	3.8
3680Å	He ₂	$11m ns^3\Sigma_u^+ \rightarrow 2p^3\Pi_g$	15.0%	5.4
3130Å	He ₂	$11m np^1\Pi_g \rightarrow 2s^1\Sigma_u^+$	17.7%	6.3

b) Pulse duration -- The pulse duration is more difficult to estimate from theory. In the first approximation the entire energy available to the lasing transition can be assumed to be emitted in a time comparable to the inverse of the recombination rate. Problems result from the paucity of measurements of this rate for collisionally-stabilized recombination. For theoretical reasons, the effective two-body recombination rate coefficient, defined for the ion X^+ by

$$\frac{\partial}{\partial t} [X^+] = -\alpha [X^+] [e] \quad , \quad (1)$$

is expected^{2,7} to have the form

$$\alpha = K_e [e] (T_e/300)^{-9/2} + K_N [X] (T_e/300)^n \quad (2)$$

where $[e]$ and $[X]$ denote the concentrations of free electrons and neutral atoms respectively, T_e , the electron temperature, and α is a coefficient which is undetermined at the present time.

Values in the literature^{7,8,9} are somewhat scattered and entirely confined to values of electron and neutral particle densities several orders of magnitude below those now obtainable with beam-excited discharges. In the absence of more appropriate values, the best estimates for He⁺ from the literature would seem to be

$$\alpha \approx 7 \times 10^{-20} [e] (T_e/300)^{-9/2} + 10^{-27} [\text{He}] \quad , \quad (3)$$

and for He₂⁺

$$\alpha \approx 1.5 \times 10^{-20} [e] (T_e/300)^{-9/2} + 1.5 \times 10^{-27} [\text{He}] \quad . \quad (4)$$

However, there is some evidence¹⁰ that a more generalized model is necessary and best parameterized as

$$\alpha = K[e]^\eta (T_e/300)^{-9/2} \quad (5)$$

where η is a function of pressure and $0 \leq \eta \leq 1$. At 44.6 Torr prior measurements over the range, 10^{10} to 10^{12} cm^{-3} , of electron densities for He₂⁺ indicated a value of

$$\alpha \approx 2.8 \times 10^{-11} [e]^{0.185} \quad (6)$$

where $[e]$ is again the electron density in units of cm^{-3} .

In either case an equivalent exponential lifetime against recombination, τ , can be defined to be

$$\tau^{-1} \equiv \frac{1}{[X^+]} \frac{\partial}{\partial t} [X^+] = -\alpha[e] \quad . \quad (7)$$

The resulting expected lifetimes are summarized in Table II.

Table II
Lifetimes Against Recombination

Species	[e] (cm ⁻³)	T _e (°K)	τ (sec)
He ⁺	10 ¹⁶	300	0.14 x 10 ⁻¹²
		3000	0.44 x 10 ⁻⁸
He ₂ ⁺	10 ¹⁶	300	1.0 x 10 ⁻¹²
		3000	3.0 x 10 ⁻⁸

Superficially it appears any lifetime and hence pulse duration could be attained provided 1) the ionization could be produced in a time short compared to the output pulse and 2) the electron temperature could be adjusted to a sufficiently low value in the same time. Unfortunately the electron temperature is not a free parameter, but is predicted^{11,12} to be controlled by the feedback of energy to the electron gas during the stabilizing collisions between excited states and the free electrons. Current theory¹¹ indicates a value in the range 1500° - 1800°K would be appropriate for the 10¹⁶ cm⁻³ electrons in helium at STP. Nevertheless it must be recognized that such an estimate is based upon extrapolation of parameters over so many orders of magnitude from measured values as to render the nine-halves power of the result to be of questionable value.

- c) Efficiency -- Although the quantum efficiencies summarized in Table I are not extremely impressive, the system efficiencies expected for a

recombination laser should be limited primarily by these quantum efficiencies. This results from an exceedingly effective use of electron beam energy. Whereas in most e-beam excited laser systems, including N_2 and H_2 , waste of over 90% of beam energy lost in inelastic collisions occurs in the production of ionization as opposed to excitation, in the recombination scheme, use is directly made of that ionization. The minor occurrence of direct excitation appears as waste in the postulated system. Considering that about 42.3eV of beam energy is expended in the production of a 24.5eV He^+ ion or 22.4eV He_2^+ ion, system efficiencies of 58% and 53%, respectively, of the quantum efficiencies should be attainable. This implies that recombination lasers should achieve overall efficiencies of 5 to 10 per cent.

Nevertheless, at the point of inception of the research reported here virtually all predictions were based on extrapolations of parameterizations of recombination processes obtained from studies at neutral pressures not substantially greater than 0.1 atmosphere and electron densities less than 10^{12} cm^{-3} . As expected, the fastest recombination lifetimes reported had been of the order of tens of microseconds.

III. EXPERIMENTAL METHOD

The objective of this program has been stated to be the evaluation of the potential utility to laser development of recombining high pressure helium plasmas. There are several ways in which this could have been done depending upon the actual characteristics such plasmas are found to have. In the preceding material these parameters were estimated theoretically on the basis of constants obtained from measurements spanning variable ranges many orders of magnitude below those of interest for this study. Should those extrapolations prove valid one would have needed only to build the laser and study the dependence of its power density on operating parameters. In fact the extrapolated values are such that the most likely pair of quantum levels for lasing could be found by simply observing which levels superradiate during the afterglow period following the ionizing pulse applied at the pressure giving the highest total ionization. If, however, higher order terms which are not theoretically appreciated tend to interfere with the realization of the extrapolations, then these higher terms would need to be determined before optimization of the parameters could be attempted.

In either case, the initial steps most clearly indicated have been the construction of an electron beam-excited, high pressure afterglow system followed by a survey of the time-resolved, spectrally resolved radiation from the plasma. The first can be conveniently considered from two aspects, plasma production and data acquisition. These together with a characterization of the resulting systems are reported below. The subsequent spectral survey is considered in the following section.

- a) Plasma Production -- Figure 3 shows an overall view of the evolved design of the plasma system and e-beam gun. The first of the high pressure afterglow chambers (HPAC-1) is shown in the center of photograph. It is basically a welded stainless steel box having the schematic form of a horizontal cross with an additional downward leg serving as an inlet port. One pair of opposed arms is terminated by gasketed windows and the other pair contains the pumping port opposite to the e-beam window. Dimensions and construction details are found in Figure 4.

HPAC-1 was of limited utility and served to facilitate expeditious testing of measurement concepts concurrent with the design and fabrication of the more sophisticated chambers HPAC-2 and HPAC-1b. Principal limitations on HPAC-1 resulted from the following factors:

- 1) Study over a large pressure range was precluded by the relatively large span of the 1 mil e-beam window.
- 2) Gas purity was limited by the gasketed construction of the windows which did not allow a complete bakeout and evacuation before back-filling with the high-pressure helium.
- 3) Precise optical measurements were limited by the lack of Brewster angle windows.

As was planned, the limitations on HPAC-1 completely determined system performance during the first six month period of the investigation.¹³ However, the remainder of the ultra-high vacuum and gas inlet manifolds were designed in a manner consonant with design projections for other highly evolved systems anticipated in later

Figure 3

Photograph of HPAC-1 (center) together with the electron beam gun to the left and the near-confocal optical cavity to the front and rear center.

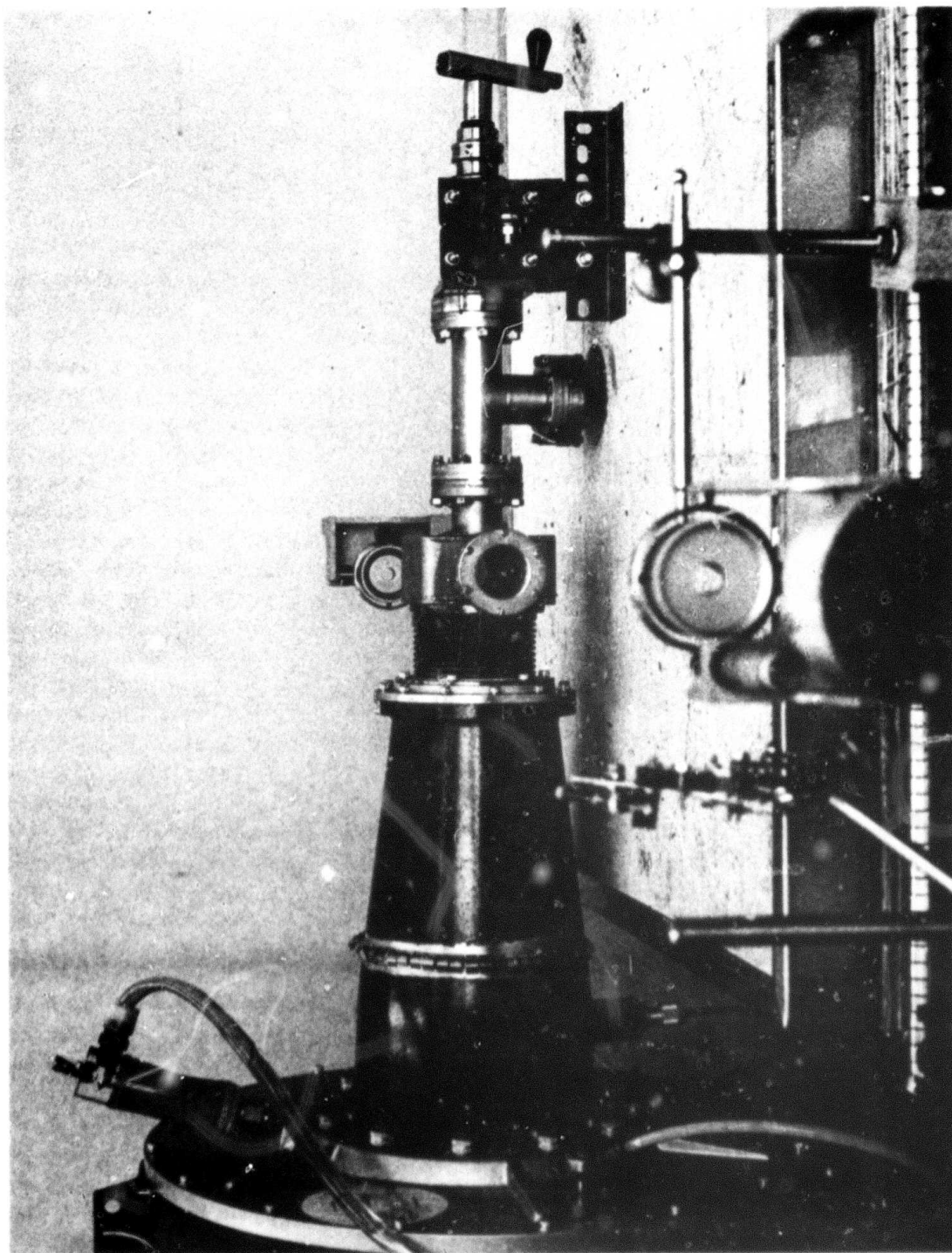
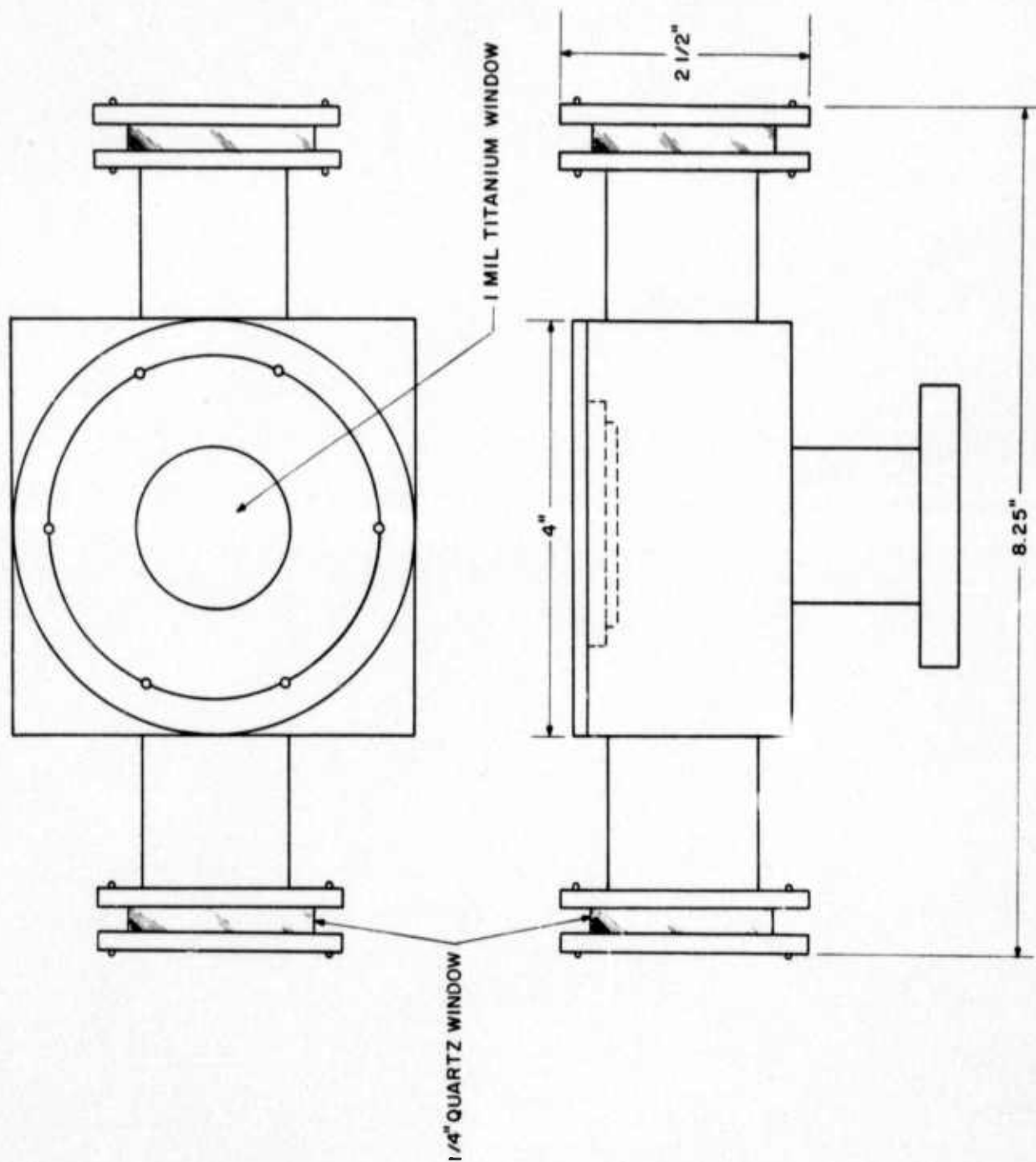


Figure 4

Drawing of the High Pressure Afterglow Chamber (HPAC-I)
showing construction details.

22.



stages of the program. Figure 5 shows a view of the vacuum and gas handling system and Figure 6 schematically outlines its functions. All standard components were Varian 2 in. UHV grade. The portion enclosed in dotted lines was bakeable to 400°C while the part in dashed lines was an addition implemented with HPAC-2 and used subsequently with HPAC-Ib to provide accurate pressure measurement without contamination.

System integrity was such that after a mild bakeout with heating tapes a pressure of 2×10^{-8} Torr could be maintained in the dump tank while the valve to HPAC-1 was open. Final verification was obtained with a commercial helium leak detector which failed to show any detectable leaks.

Restriction 1) on the pressure range was removed in principle with the design of HPAC-2. The span of the e-beam window was reduced to a value theoretically appropriate for operation at 20 atmospheres. Nevertheless a considerable sequence of mechanical failure was encountered and it was finally deemed inappropriate to continue with that particular subcontractor. To minimize loss of productive time a modified version of the first cell, HPAC-Ib was fabricated for use to 5 atmospheres, but with restrictions 2) and 3) removed. Concurrent with this step facilities were being established to build future high-pressure cells "in-house". These have been completed at the end of this reporting period and it is anticipated that a completely redesigned cell HPAC-3 will be available in the near future.

Figure 7 shows a drawing of HPAC-Ib. Construction details are entirely similar to HPAC-1 with the exception of the optical windows.

Figure 5

Photograph of the e-beam gun and HPAC-1 to the left, front
and the UHV vacuum support system to the rear.

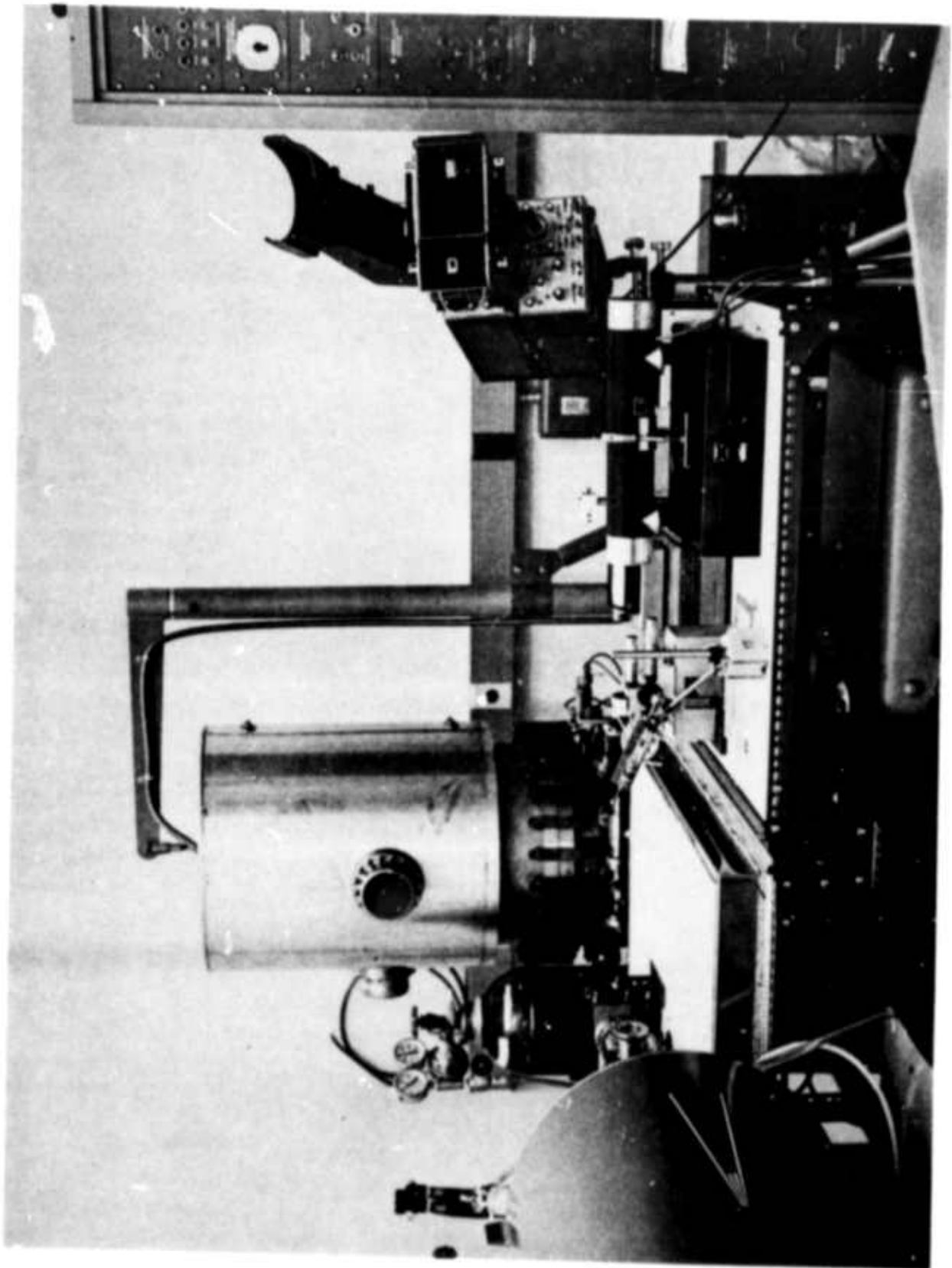


Figure 6

Schematic representation of the UHV vacuum and associated gas handling systems. The dotted lines enclose portions bakeable to 400°C. The dashed lines enclose additions to the system to be implemented when HPAC-2 was installed and used subsequently with HPAC-1b.

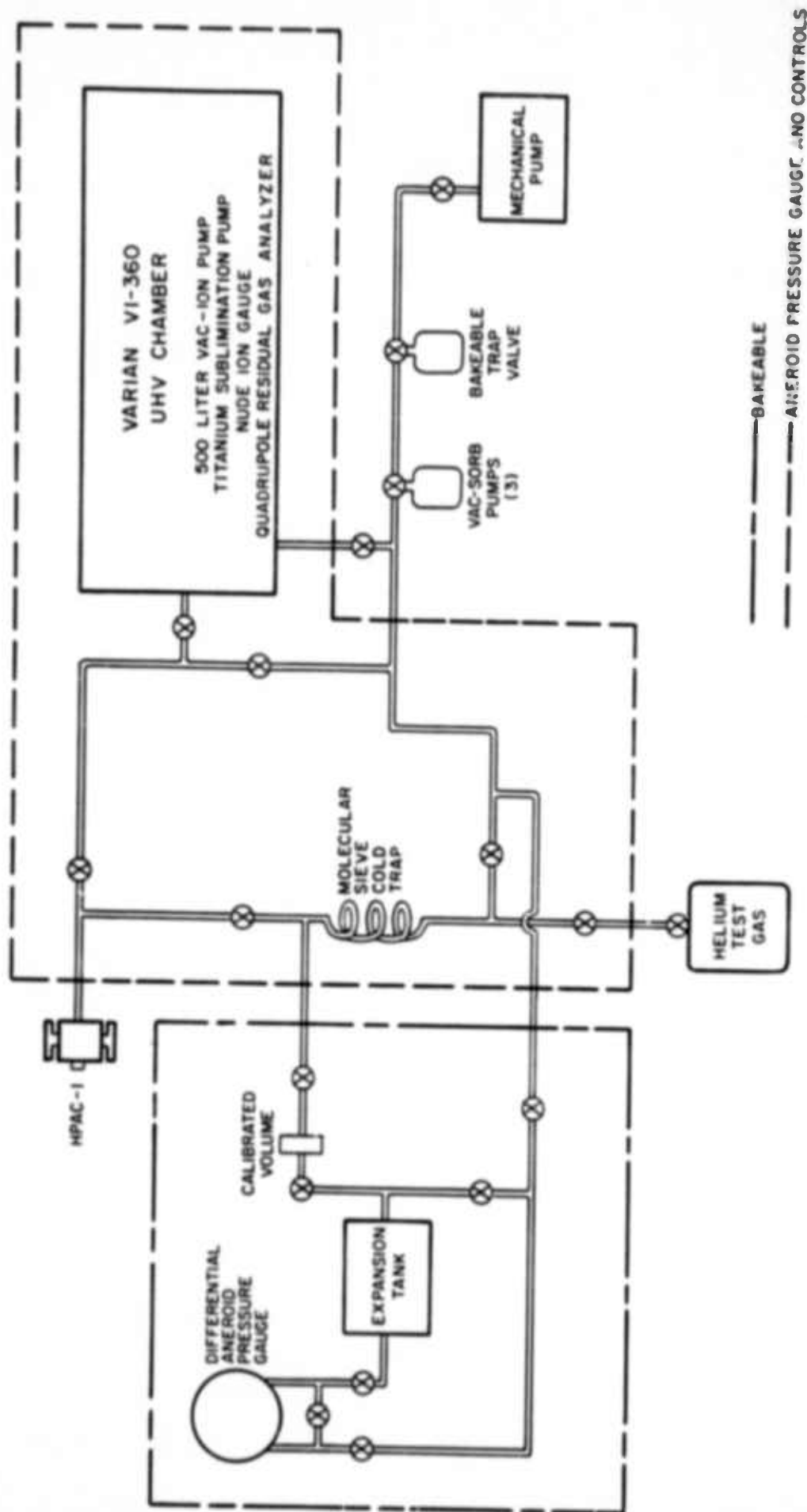
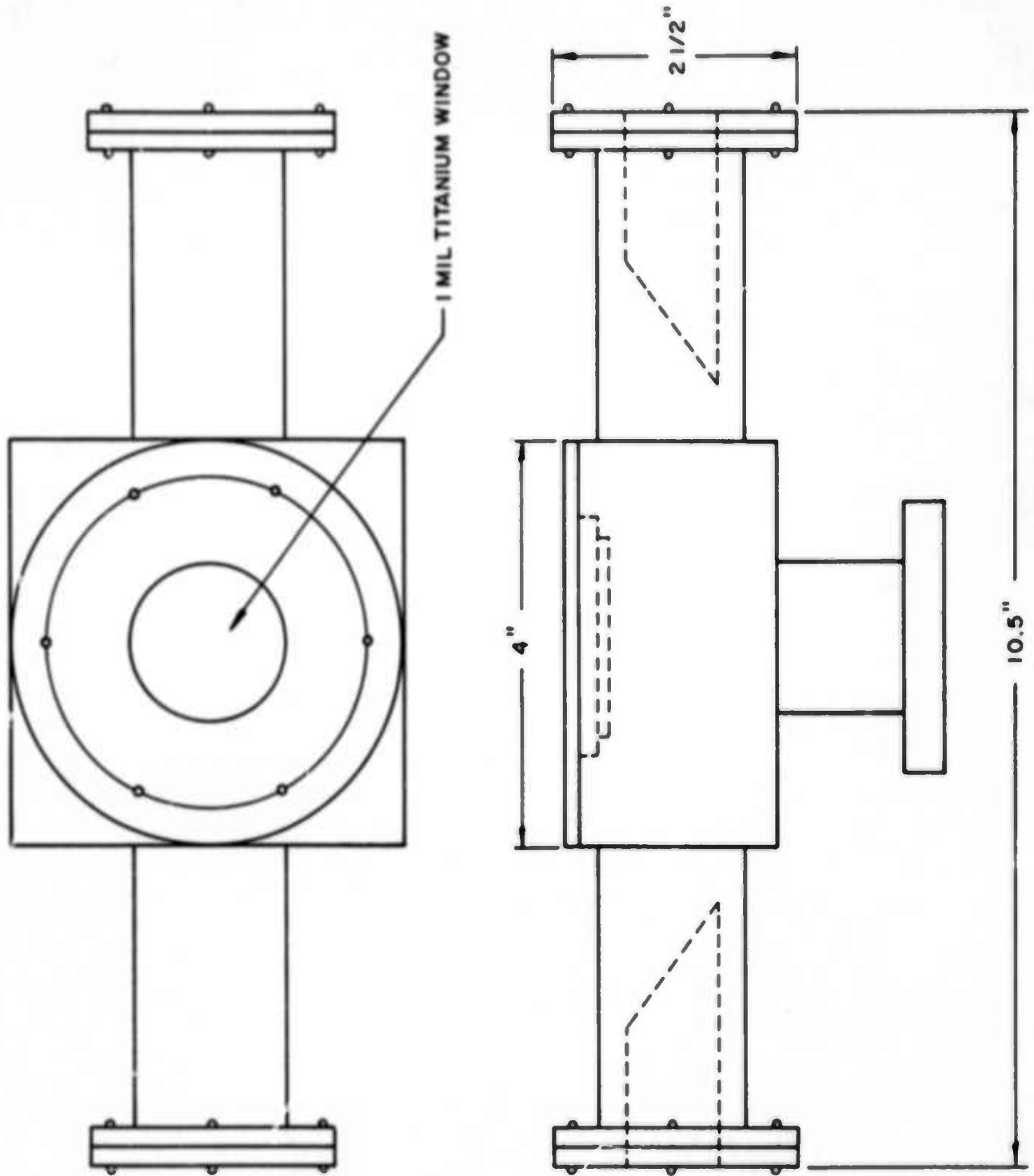


Figure 7

Drawing of the High Pressure Afterglow Chamber, Version 1b
(HPAC-1b) showing construction details.



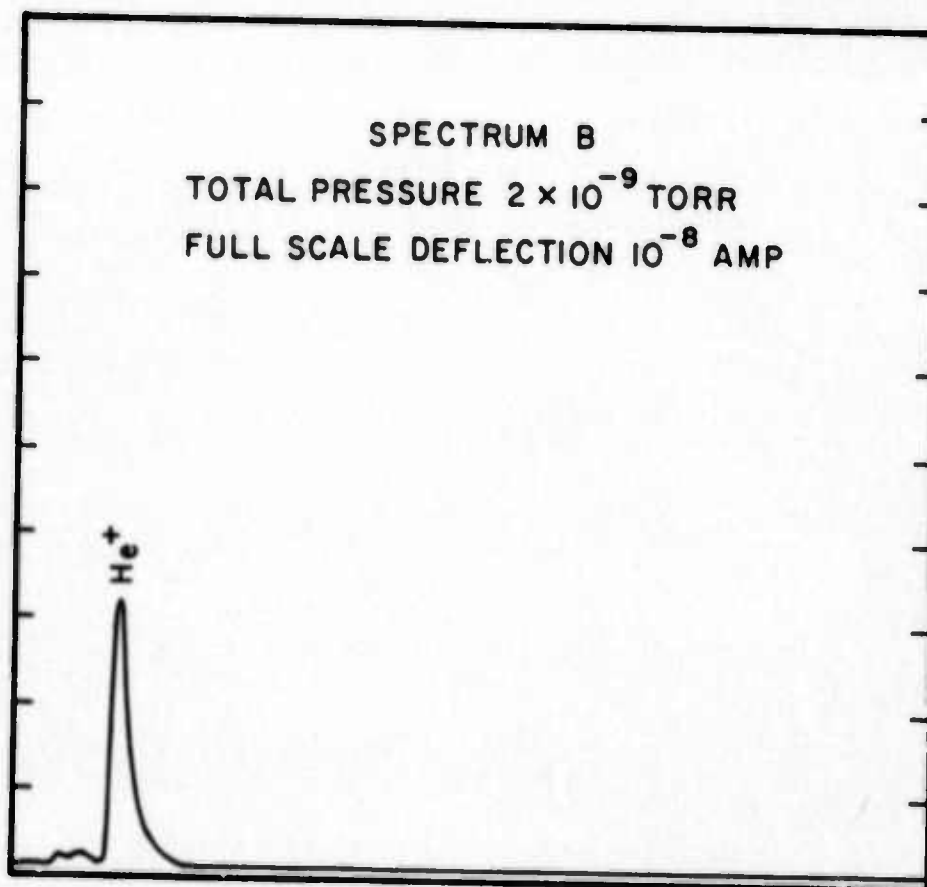
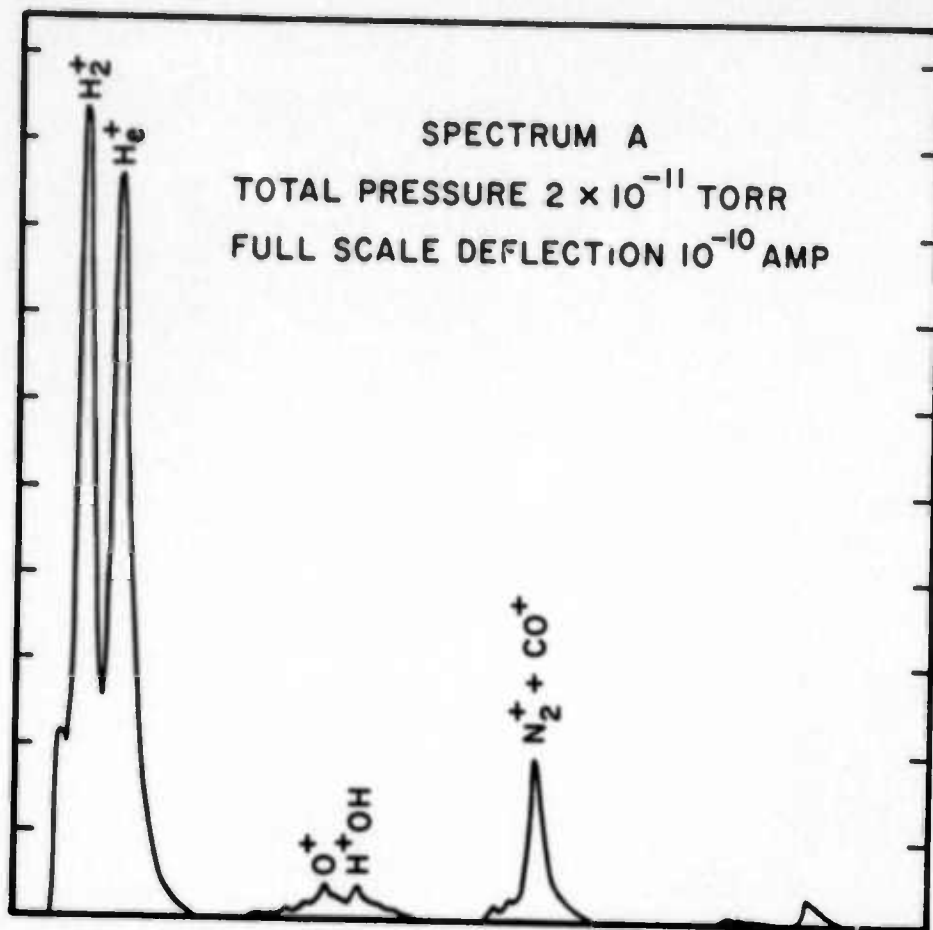
Quartz windows were fused to quartz tubing cut at the Brewster angle and these joined through graded seals to Varian UHV flanges. With this arrangement system integrity was complete as evidenced by the fact that after a mild bakeout to 300°C a pressure of a few $\times 10^{-11}$ Torr could be maintained in the dump tanks. Residual gas analysis was performed after each evacuation and showed only traces of contaminant. A typical mass spectrum is shown in Figure 8a.

After evacuation, the chamber was valved off from the pump and filled through the inlet port with helium of high initial purity, further conditioned by passing it at the fill pressure through a molecular sieve trap cooled to liquid nitrogen temperatures. Bureau of Mines analyses of cylinders of similar grade have shown one or two ppm non-condensable, inert (neon) impurity and it is believed that this figure represents the ultimate purity attainable with this system. As will be discussed in the following section, this treatment sufficed to reduce all impurities below the threshold of spectroscopic detection by optical means. Typical mass spectrometric analysis of the cell contents at the completion of an experimental sequence is shown in Figure 8b. No evidence of leakage or gas evolution can be detected. Nevertheless, should the need arise in future stages, several cylinders of <0.2 ppm inert impurity have been obtained. Further improvement to parts in 10^9 can be achieved if necessary through low-pressure cataphoresis followed by recompression. This latter is a tedious and expensive step and will be implemented only if necessary.

Figures 8

Residual gas analysis obtained after evacuation of HPAC-1b

- a) Mass spectrum of steady state evacuation, initial condition before filling with helium.**
- b) Mass spectrum of cell contents after an experimental cycle of the order of 4 hours and 50 e-beam discharge pulses.**



In each cell the primary ionization is produced by a nominal 0.5 MeV electron beam entering the HPAC through a 0.001 inch thick titanium foil. The beam is produced by a Field Emission Corp. 706 e-beam gun which can emit 2×10^{14} electrons per 3-nanosecond pulse. Divergence of the beam is reported to be 30° so that at a distance l , normal to the window, there can be expected to be

$$N_p = 1.5 \times 10^{14} [1 + 0.81l + 0.165l^2]^{-1}, \quad (8)$$

primary electrons per cm^2 incident upon the HPAC beam window. From values of average range, energy expended per ion-electron pair, and gas density, an average charge multiplication factor in helium of

$$M = 15.6 \text{ cm}^{-1} \text{ atm}^{-1}, \quad (9)$$

can be computed.

The preliminary diagnostic data obtained with HPAC-1 and discussed in the following section was obtained at a helium pressure of 3 atm. with the e-beam gun located a distance of 7cm from the afterglow chamber. For these parameters the initial helium ion concentration should be

$$[+] \sim 5 \times 10^{14} \text{ cm}^{-3} \quad \text{HPAC-1} \quad (10a)$$

Closer proximity to the e-beam gun was obtained with HPAC-1b and corresponded to an initial ion concentration at 3 atmospheres of

$$[+] \sim 1.7 \times 10^{15} \text{ cm}^{-3} \quad \text{HPAC-1b} \quad (10b)$$

For purposes of the subsequent calculation of efficiencies an expression for the input energy to the afterglow from the beam is useful. Considering the specified beam energy of 4.8 Joules and range of 450 cm/atm at the 60% power of 300 KeV, the average beam energy deposited in the plasma is

$$E_b = 7.8 \times [1 + 0.81l + 0.165l^2]^{-1} \text{ J/liter} \quad . \quad (11)$$

Better values for these parameters are contingent upon calibration of beam current and divergence, but it is believed that the interrum use of these approximations are consonant with the current allocation of priorities in this project, as well as consistent with the accuracy at this stage of investigation of the data reported in the following section.

Several instructive problems were encountered with the initial operation of the system. Both RFl and X-ray noise were extreme and extensive protective measures were necessitated. Nested enclosures were constructed to suppress counting from the innermost, the RFl, X-rays, and RFl again. The innermost enclosure consisted of a copper bellows assembly bolted to the face of the e-gun and grounding through spring contact to the mounting ring supporting the foil window. Blocking the passage in the bellows was a .004" thick Mylar disk placed to protect the face of the e-gun from the possible back ejection of material from the foil window.

Surrounding the HPAC, together with the evacuation tube and valve to the dump chamber was a 1/16" lead enclosure with open ports to allow access to the optical windows and bellows connecting to the

e-gun. Additional 0.5" lead plates were positioned in strategic locations to shadow the external instrumentation and operators.

The outermost, and most complete RF1 shield consisted of 5 sides of a welded aluminum cube approximately one meter on a side. It can be lowered onto an aluminum base plate lying under the asbestos base of the bakeout oven. Electrical contact between the case and base is assured by commercially available RF1 gasketing. All gas inlets and vacuum lines through the base were grounded to base by sealing them to the base at the point of penetration with RF1 gaskets. Contact between the penetrating tapered output end of the e-gun and the case is made with a sliding RF1 gasket. The only unprotected openings through the enclosure are the two opposed circular ports centered on the same optical axis as the windows of the HPAC. Since there are no significant asymmetries or conductive penetrations through these holes, RF1 radiated from them is at a minimum level and one which was found to be acceptable to the external instrumentation.

- b) Data Acquisition -- At this stage of investigation, the primary data is spectral. At 3 atmospheres pressure with a transverse optical axis intensities are relatively low overall. Three high-aperture spectroscopic systems have been found useful, an f/2 camera-spectrograph with about $300\text{\AA}/\text{mm}$ dispersion at the film plane, and an f/4, 0.25 meter spectrometer with the exit slit removed to give about 100\AA resolution, and an f/4, 0.25 meter spectrograph coupled to a 4-stage image intensifier system arranged so that the dispersed spectrum of a single discharge could be photographed at a sensitivity where single-photon scintillations could be recorded.

The f/2-spectrograph was employed primarily to obtain the time-integrated spectra of the e-beam afterglow for the purpose of locating features of interest, as well as serving as an impurity monitor. Four pulses at the maximum beam energy were required for a useful exposure on Tri-X film developed to an ASA equivalent index of 2400.

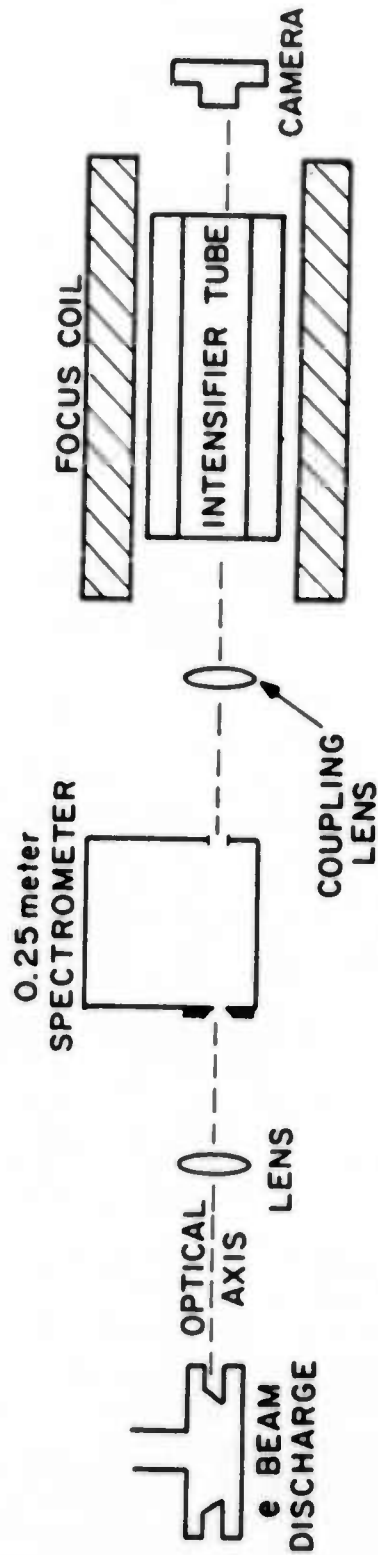
The f/4-spectrograph/intensifier shown schematically in Figure 9 was to extend both sensitivity and resolution of the f/2 survey instrument. By adjustment of the accelerating voltage threshold sensitivity could be varied from the resolution of single photon scintillations to the integral of n successive photon scintillations within the decay time of the phosphor on the output screen.

The 0.25 m spectrometer was used with a nine stage RCA-C31025C photomultiplier to obtain the transient intensity response for a particular 100\AA wavelength region. The useable region of sensitivity extended from 3000\AA to 8500\AA . The photomultiplier risetime of 1.5 nanosecond insured the transient intensity could be monitored with nanosecond resolution if adequate recording techniques were used. Intensities were such that typical signals were in the range of 0.1 to 1.0 volts into 50Ω with decay times in the range of a few $\times 10^{-8}$ sec. to a few $\times 10^{-7}$ sec.

This suggested the use of a Biomation 8100 transient recorder which provides the 8-bit digitization of input signals not less than 0.05 volts for full scale conversion over 2048 time increments of at least 10 nanoseconds each. The device was directly interfaced to the data acquisition computer currently serving the University's Atomic Physics group. Future refinements are under construction to give 300 psec resolution for at least the first 16 points.

Figure 9

Schematic representation of the spectrograph-image intensifier combination used to record spectra of single discharges at the level of sensitivity where single photon scintillations could be distinguished .



Calibration of the 0.25 m spectrometer and detection system was accomplished by comparison to a standard of irradiance traceable to NBS. Detection sensitivities which calibrated the power at the spectrometer entrance slit to voltage at the 8100 input ranged from 20μ watts/volt at 8800\AA to 12μ watts/volt at 6700\AA decreasing to 22μ watts/volt at 4000\AA . The rather low sensitivity in the violet was primarily a consequence of the 6000\AA blaze wavelength of the grating, chosen to enhance the usually depressed red-sensitivity of most fast detection systems. A consideration of geometrical factors and volume sampled gave an overall calibration depending on wavelength which equated between one and two kilowatt/liter of incoherent power radiated from the e-beam afterglow to 1 volt of detected signal.

The addition to the system of an external optical cavity containing HPAC-1 and having coincident optical axis with it has permitted the preliminary inference of optical gain from measurements of the enhancement of certain spectral features observed in the optical cavity. The cavity supporting these measurements is a sub-concentric geometry imposed by the availability of mirrors and the physical dimensions of the shielded system. The measurements discussed in the following section were obtained with multi-layer dielectric mirrors of maximum available reflectivity over the 6000 to 7000\AA region. Other mirror sets are available but detailed examinations at 3 atmospheres have been currently confined to the red region.

A preliminary characterization of the 3-atmosphere e-beam afterglow in helium was obtained during the initial 6-month period with the system as described. Extension of these results to span the one to

five atmosphere region was accomplished during the 3-month remainder of the reporting period. Results are presented in the following section. Fabrication of the more advanced HPAC-3 is in progress and the greater pressure range afforded will be coupled with a detailed examination of the recombination processes in a manner guided by the following preliminary results.

IV. TECHNICAL RESULTS

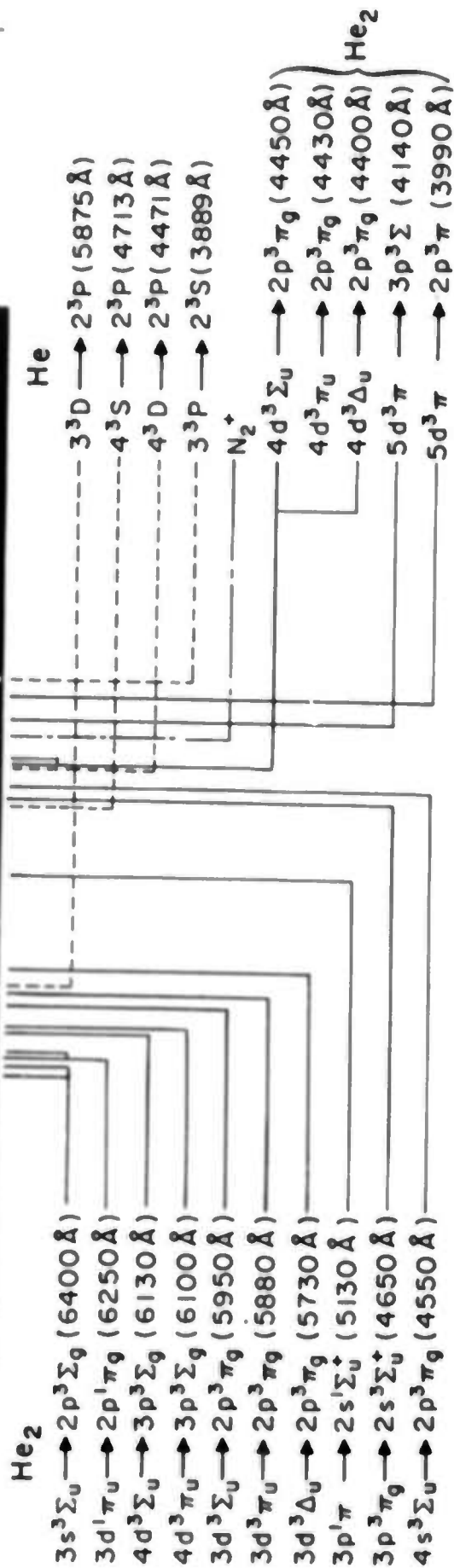
Preliminary values were obtained for the most important diagnostic parameters characterizing the e-beam afterglow excited in 3 atmospheres of helium with the previously described HPAC-1 system.¹³ Confirmation and extension of these values to cover the one to five atmosphere pressure range was accomplished in the HPAC-1b chamber at greatly improved gas purity. Parameters considered in this work were a) output wavelengths, b) recombination lifetimes and peak power levels, c) incoherent output efficiencies, and d) inferred optical gains. Each is considered in the following subsections:

- a) Output wavelengths -- Figure 10 presents a survey spectrum of the visible region made with the f/2 spectrograph. Long wavelengths are to left. The upper spectrum is a comparison spectrum of a d.c. recombination source in helium at 3 Torr. Its purpose is to provide a reference for the He₂ spectrum which is generally difficult to obtain from commercial spectral sources. The lower spectrum is a composite of four pulses of e-beam afterglow in helium at 3 atmospheres in the HPAC-1 system together with the atomic helium spectrum from a commercial source superimposed over the lower 1/3 of the strip. Exposure of the lower strip was at an aperture of f/2 on Tri-X film developed to an equivalent ASA index of 2400. The appearance of the upper, reference, He₂ spectrum is what would be considered "regular" in the literature being characteristic of a cool (~500°K) recombination spectrum of He₂⁺ at about 10¹¹ electrons/cm³ and a negligibly low neutral gas pressure.

Figure 10

Survey spectrum of the visible region made with an $f/2$ spectrograph. Long wavelengths are to the left. The upper spectrum is a comparison spectrum of a d.c. recombination source in helium at 3 Torr. The lower spectrum is a composite of four pulses of the e-beam afterglow in helium at 3 atmospheres in the HPAC-1 system and the atomic helium spectrum from a commercial source superimposed over the lower 1/3 of the strip. Exposure of the lower strip was at an aperture of $f/2$ on Tri-X film developed to an equivalent ASA index of 2400.

Upper Spectrum - 3 Torr Helium recombination
 Lower Spectrum - 3 atm. e-beam afterglow in Helium (full height)
 Atomic Helium calibration source (lower 1/3)



Principal features have been identified below the spectra and term values referenced can be identified from Figure 2. If the intensities of the spectrum of the e-beam afterglow are qualitatively normalized to the usually dominant emissions from the reference spectrum of He_2 , namely the triplet 3d complex at 5950, 5880, and 5730Å, then the following transitions appear anomalously enhanced:

1. the $3s^3\Sigma_u^+ \rightarrow 2p^3\Sigma_g^-$ at 6400Å
2. the $3d^1\Pi_u \rightarrow 2p^1\Pi_g$ at 6250Å and
3. the transitions from the 4d complex to the po level at 6130 and 6100Å.

Remaining bands appear at relative intensities which could be reasonably expected from radiative and collisional cascading in the course of the stabilization of the collisional-radiative recombination of He_2^+ . This is the cascading discussed in Section II. Of course such comparisons are quite qualitative and dependent upon subjective average over a considerable variety of low pressure helium recombination spectra. Nevertheless, the three features cited above are quite enhanced.

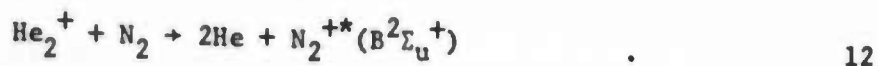
The first and third represent transitions which in a sense compete with the normally intense 3-d complex. As can be seen from Figure 2, the third is equivalent to a short-circuit from principal quantum level 4 to 2 bypassing the "normal" stabilization current which tends to relax captured electrons from one principal quantum level at a step. The first can be rationalized as a transition from a state benefitting from one of the "fine-tuning"

effects of collisional stabilization which tend to move bound electron populations back and forth between angular momentum sub-levels corresponding to the same principal quantum number. It is this effect which, as discussed in Section II, would allow a lasing transition to capture virtually all of the stabilizing electron current between principal quantum levels. In the case of the 6400\AA transition the particular radiating sublevel lies at a somewhat lower energy, $\sim 0.22\text{eV}$, than the d-complex and should show a gain of population relative to the d-complex when the electron density is high and such "lateral" collision are frequent.

No such ready explanations appear for the enhancement of the singlet feature and underscore the caution with which all such a priori interpretations of the preliminary data must be viewed. In fact, subsequent study showed this band was enhanced by a contribution from second order emission from the OH radical. Spectra obtained from the HPAC-1b system showed this singlet feature to appear from recombination at its "normal" relative intensity suggesting no preferential enhancement. The remaining first and third features are not inconsistent with the gross adjustments expected for the collisional recombination processes in the course of extrapolation over orders of magnitude of electron density.

Also evident in Figure 10 are other serious impurity problems. The relatively prominent feature around 4300\AA is clearly a member of the First Negative series of N_2^+ . This is a selectively enhanced series generally excited in helium afterglows¹⁴ by the charge trans-

fer reaction



It provides a very sensitive test for air leakage and evidences one of the difficulties encountered in using the gasketed HPAC-1 system.

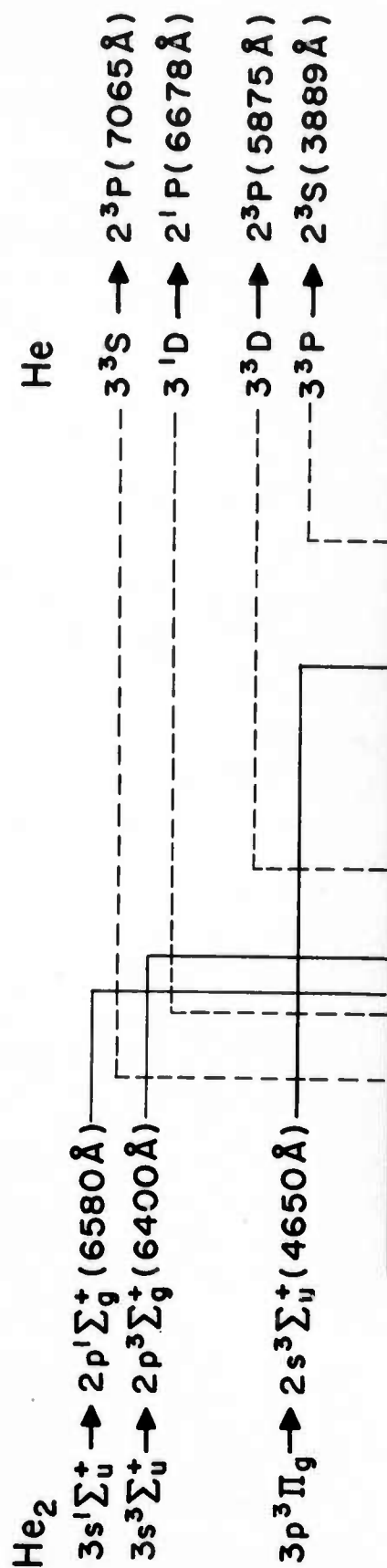
An instructive problem was encountered in the interpretation of the spectral data of Figure 10 in that it was known that the particular film which had been used suffered from a sharp cut-off of sensitivity somewhere in the region of 6400Å. This is in fact suggested by the virtual absence of features to the red of the 6400Å band.

Figure 11 shows the same spectra as Figure 10 with two exceptions, (1) the reduction of contaminants, and (2) the use of Eastman 2485 film with extended red sensitivity developed to an ASA index of 8000. There is, of course, an immediately evident problem in that forcing the film speed has cost the extensive diffusion of the image. A more subtle problem is that the high resulting gamma of the film makes it an approximate square-law detector in which a proportionate increase in incident intensity is recorded as a squared increase in film density. Nevertheless, the extreme enhancement of the 6400Å is now quite obvious, resulting from either the greatly reduced insensitivity of the film at this wavelength, or the lack of possible quenching by impurity molecules.

In addition the analogous singlet band $3s^1\Sigma_u^+ \rightarrow 2p^1\Sigma_g^+$ at 6590Å is seen to be strongly enhanced. The atomic lines at 7065Å, $3^3S \rightarrow 2^3P$; 6678, $3^1D \rightarrow 2^1P$; join the 5875Å transition, $3^3D \rightarrow 2^3P$ as being the

Figure 11

Survey spectrum of the visible region made with an $f/2$ spectrograph on film with extended red sensitivity. Long wavelengths are to the left. The lower spectrum is a comparison spectrum of a d.c. recombination source of helium at 3 Torr. The upper spectrum is a composite of four pulses of the e-beam afterglow in helium at 3 atmospheres in the HPAC-1 system and the atomic helium spectrum from a commercial source superimposed over the upper-middle $1/4$ of the strip. Exposure of the upper strip was at an aperture of $f/2$ on Eastman 2485 film developed to an ASA index of 8000.



-48-

Upper Spectrum - 3atm e-beam afterglow in Helium (full height)
Atomic Helium calibration source (short lines)

Lower Spectrum - 3 Torr Helium recombination

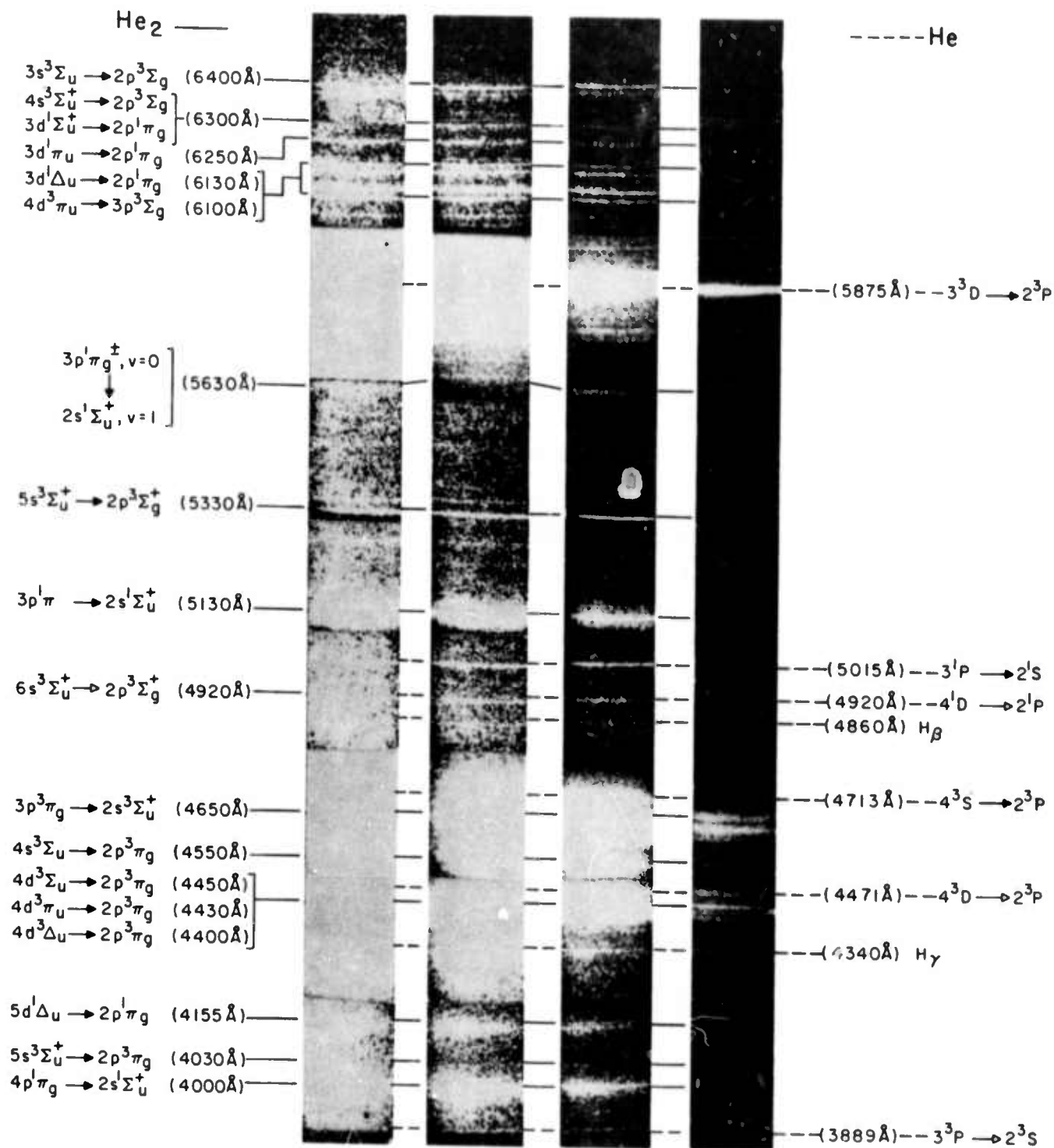
only atomic lines of appreciable intensity. In this figure the superimposed reference spectrum covers the top 1/3 of the strip. The possible cause for enhancement of these three atomic helium lines or the converse quenching of all others remains obscure. As will be discussed in the following material each, in addition, shows an anomalous lifetime.

Calibration of the film against exposures of the standard lamp were attempted but the reciprocity failure of the film made the results of doubtful value. The photoelectric measurements discussed below fixed the peak power of the 6400\AA feature to be of the order of 1000 watts/liter, a value found to be about half the corresponding intensity of the 5875\AA peak. The greater apparent brightness of the figures of the latter is a consequence of its much greater lifetime.

Figure 12 presents a survey spectrum of a single discharge in the HPAC-1b system made with the f/4 spectrograph-image intensifier combination having greatly improved sensitivity and resolution. Principal limitation on both quantities have been reduced to the quantum noise imposed by the discrete nature of the photodetection events. All the information available in the spectrum has been recorded. Primary detection occurs with an S-11 photocathode with subsequent acceleration and multiplication of the emitted photoelectrons. In contrast to the direct film recordings of Figures 10 and 11, this system has an enhanced sensitivity in the shorter wavelength region and a pronounced cut-off in the red around 6400\AA .

Figure 12

Survey spectrum of the visible region made with the f/4 spectrograph - image intensifier system. Long wavelengths are to the left. Each spectrum is a time-integrated record of the afterglow from a single discharge of the e-beam gun in helium at 3 atmospheres in the HPAC-1b system. Exposures are for different accelerating voltages corresponding to different values of the number of superimposed photon scintillations required within the decay time of the output phosphor to reach the threshold for photographic detection. From top to bottom, accelerating voltages are 25, 30, 35 and 40 KV, the last two satisfying the requirements for the detection of scintillations from single photoelectrons.



Relative sensitivity of the intensifier tube as a function of wavelength is shown in Figure 13.

Several exposures of the spectrum are shown in Figure 12 and correspond to different values of accelerating voltage on the image intensifier tube and, hence, to different values of gain for the photoelectron amplification. Each represents a different value of the number of successively superimposed photon scintillations required within the decay time of the output phosphor to reach the threshold exposure of the recording film. From top to bottom the exposures represent increasing accelerating voltage with the last two strips satisfying the requirements for the detection of scintillations from single photoelectrons. Values of actual photoelectron gain corresponding to the accelerating voltages shown can be read from Figure 14.

Because of its greater resolution, Figure 12 serves to provide more positive identification of the features of the survey spectra from HPAC-1. Most of the He₂ spectrum is seen, again with principal interest being directed toward the relatively enhanced features in the red. However, now can be seen that the other members of the "favorable" Rydberg-series discussed in the introductory material are present. In particular

1. the $ms^3\Sigma_u^+ \rightarrow 2p^3\Pi_g$ series convergent at 3680\AA is represented strongly by the $m=3,4$ and 5 members at 6400\AA , 4540\AA and, 4030\AA , respectively, and

Figure 13

Graph as a function of wavelength of the relative sensitivity of the image intensifier system used to obtain the data of Figure 12.

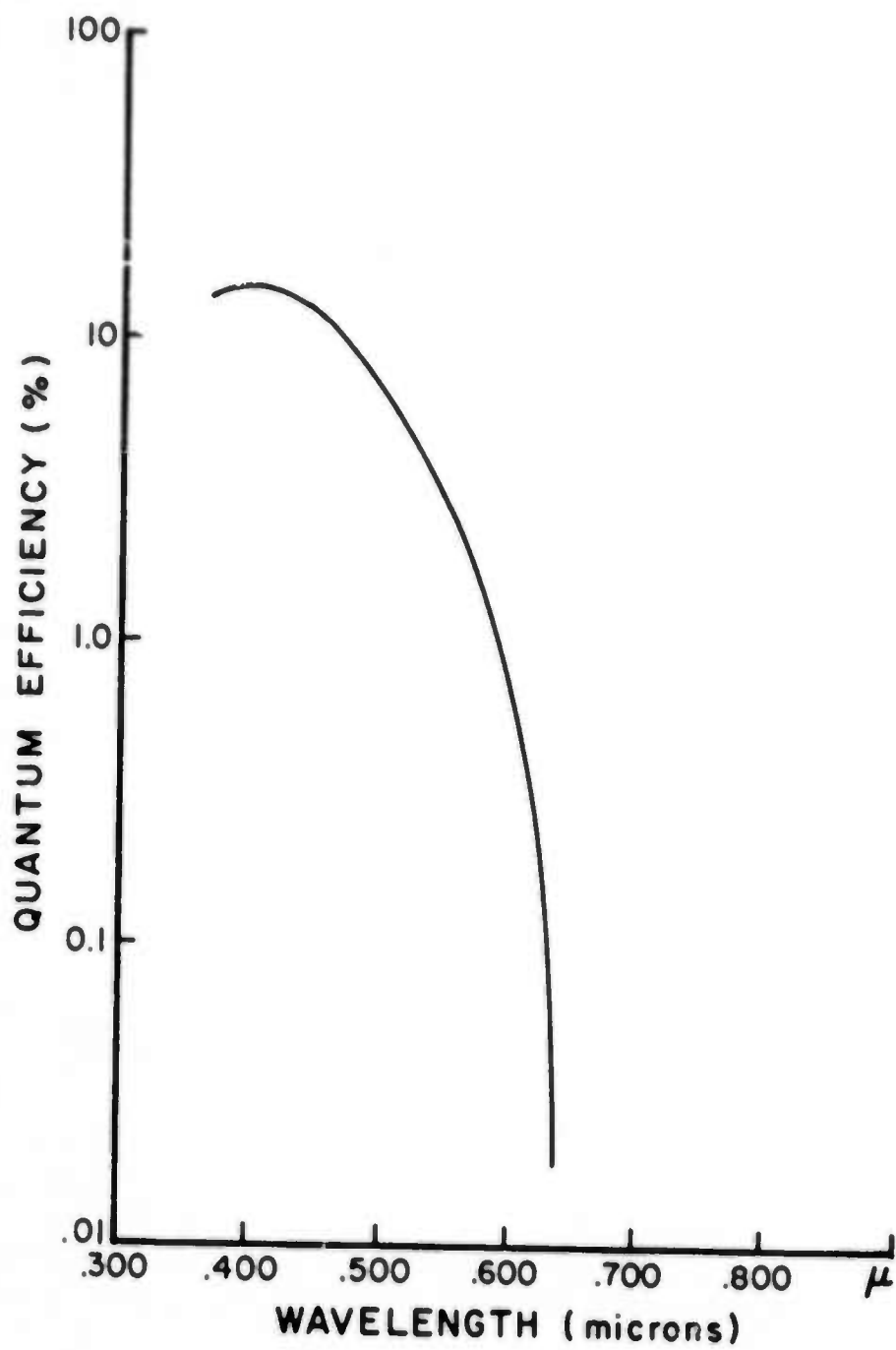
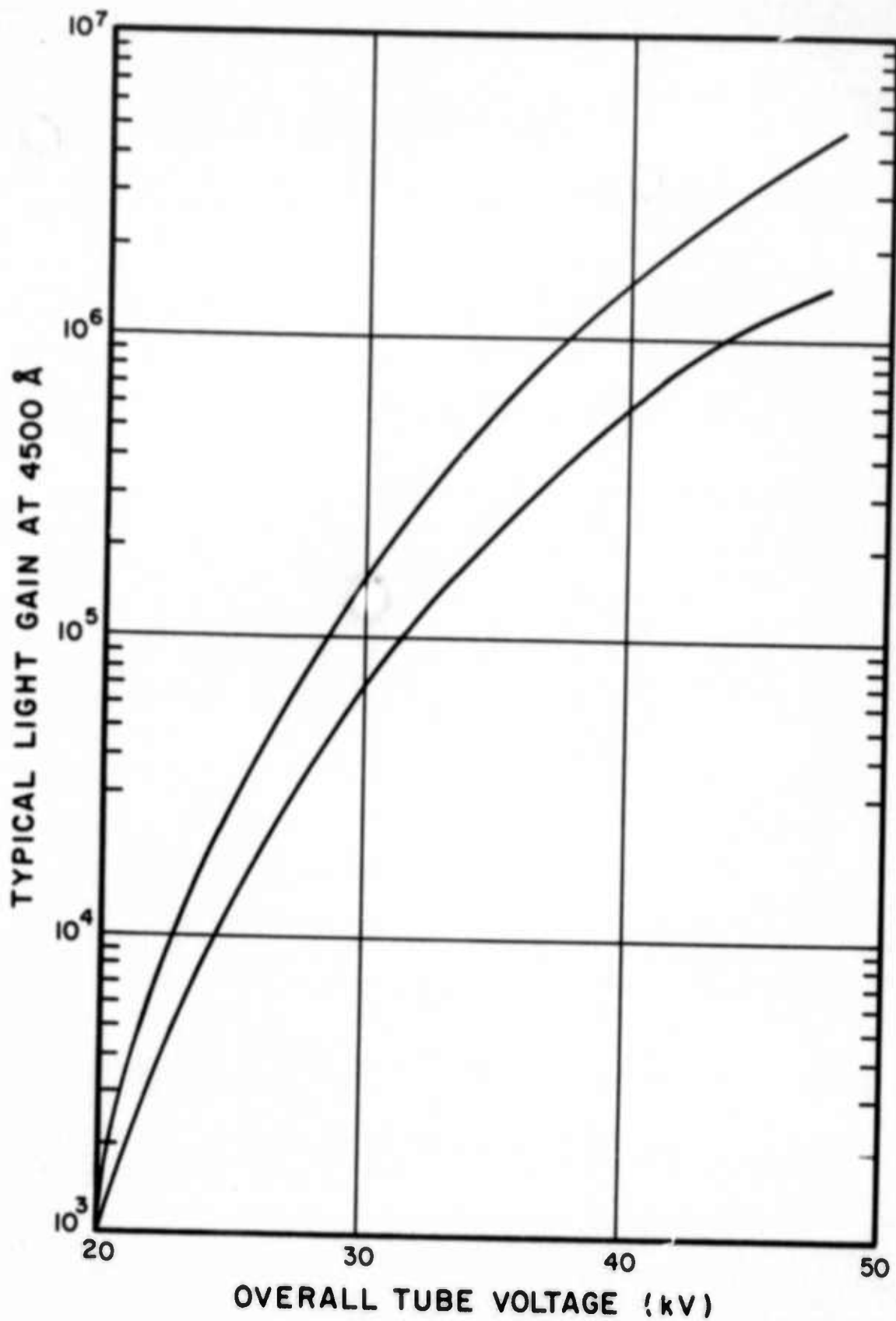


Figure 14

A graph of photoelectron gain as a function of accelerating voltage for the image intensifier system used to record the spectra of Figure 12.



2. the $mp^1\Pi_g \rightarrow 2s^1\Sigma_u$ convergent at 3130\AA and terminating on a state optically connected to the $1s\sigma^22s\sigma$ repulsive ground state is evidenced by the relatively strong $n=3$ and 4 components at 5130\AA and 4000\AA respectively. This latter series is of tangential interest in that if lasing could be accomplished for one component the delivery of population to the $2s^1\Sigma_u$ state might occur at a rate sufficient to invert the vacuum - UV transition from this state to the repulsive ground state.

The spectral information of Figure 12 is summarized in Figures 15 and 16 which are energy levels diagrams of He and He_2 in which for clarity only those states participating in transitions observed in the afterglow with appreciable intensity are shown. The general observation can be made that the abundance of He_2 levels excited is characteristic of a collisional-radiative recombination origin of the light with good collisional mixing between levels. The rather restricted excitation of the He spectrum is, conversely, more characteristic of some type of selective excitation and warrants further investigation of the possible kinetic processes which might supply such upper state excitation.

Figure 15

Energy level diagram of atomic helium showing for clarity only those states participating in transitions observed with appreciable intensity in the afterglow at three atmospheres.

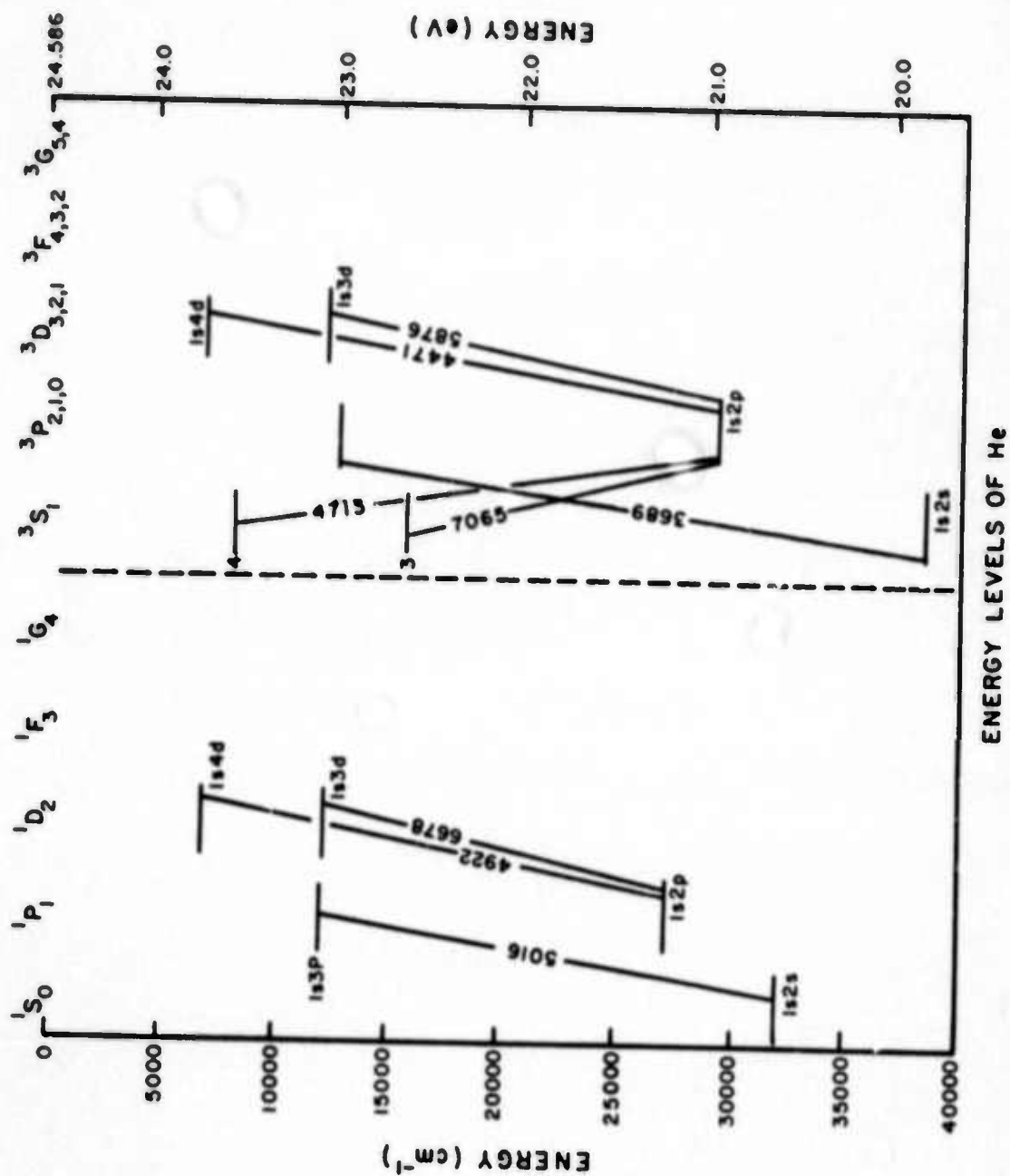
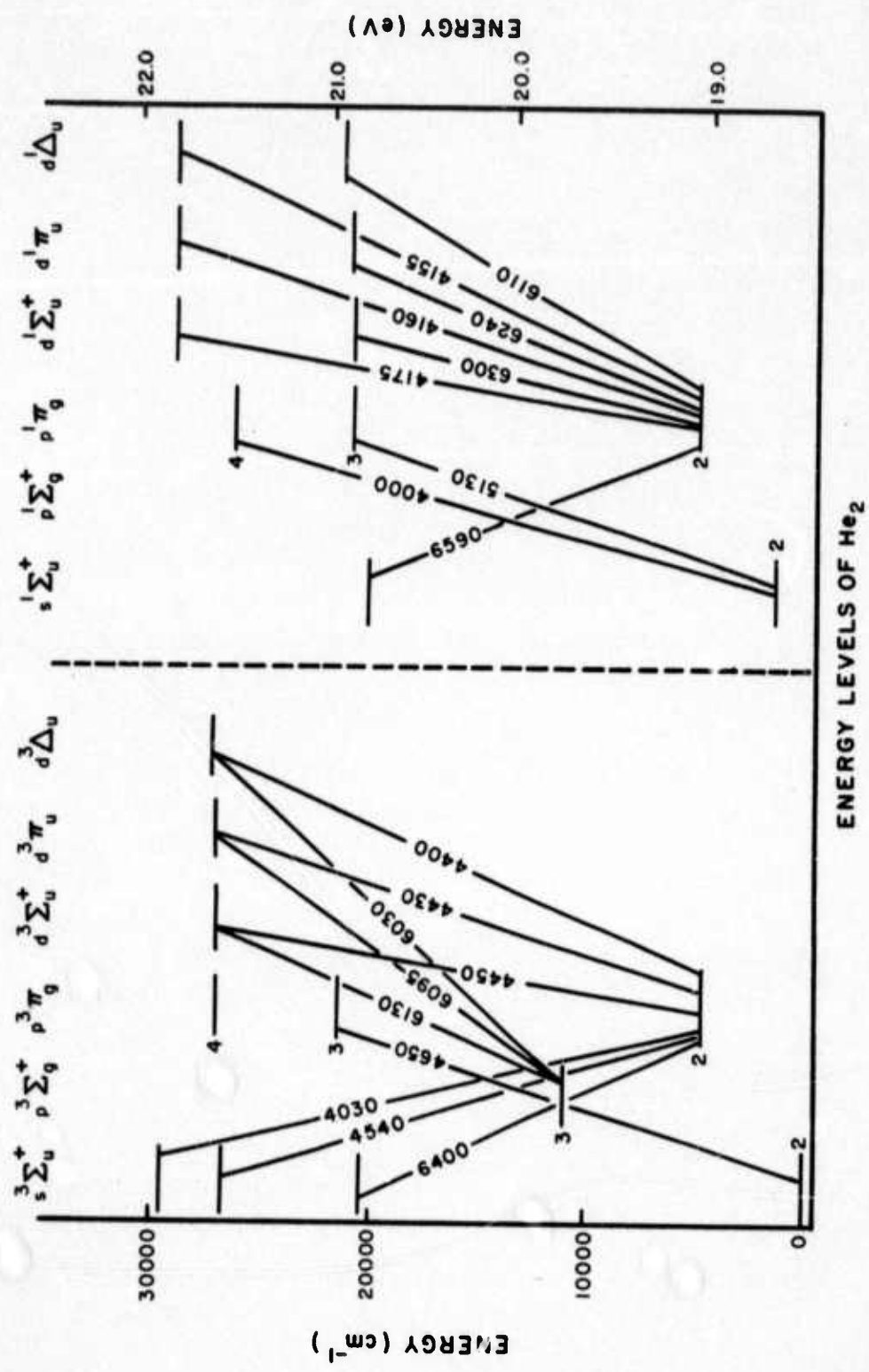


Figure 16

Energy level diagram of molecular helium showing for clarity only those states participating in transitions observed with appreciable intensity in the afterglow at three atmospheres.



- b) Recombination lifetimes and peak power -- Figure 17 shows a reconstruction of the time evolution of a single pulsed excitation of the 6400\AA feature in the e-beam afterglow at 3 atmospheres in the HPAC-1 system. Displayed is the scope output of the transient recorder which consists of continuously refreshed replays of the stored transient. As discussed, a direct connection of a data acquisition computer was also available to allow for the output of the digital image of the stored transient.

Scale of the data of Figure 17 is 200 nanoseconds per horizontal division and 270 watts/liter per vertical division. This particular feature tended to saturate the photomultiplier and the data shown was obtained with a 1.0 neutral density filter, the scale being adjusted accordingly. As will be seen this general type of decay was found to be typical of the recombination emission from the He_2 systems.

To determine the apparent functional form of direct excitation of the radiating level during the 3 nanosecond e-beam pulse, observation was attempted of the transient emission from a state optically connected to the ground 1^1S state of atomic helium. The ground $1s^2 2s^2 (1\Sigma_g^+)$ state of He_2 is strongly repulsive and unavailable for direct excitation. Figure 18 shows the resulting measurement of the emission of the $3^1\text{P} \rightarrow 2^1\text{S}$ transition in atomic helium at 5015\AA . The horizontal scale is again 200 nanoseconds per division and the vertical scale is 25.6 watts/liter per vertical division,

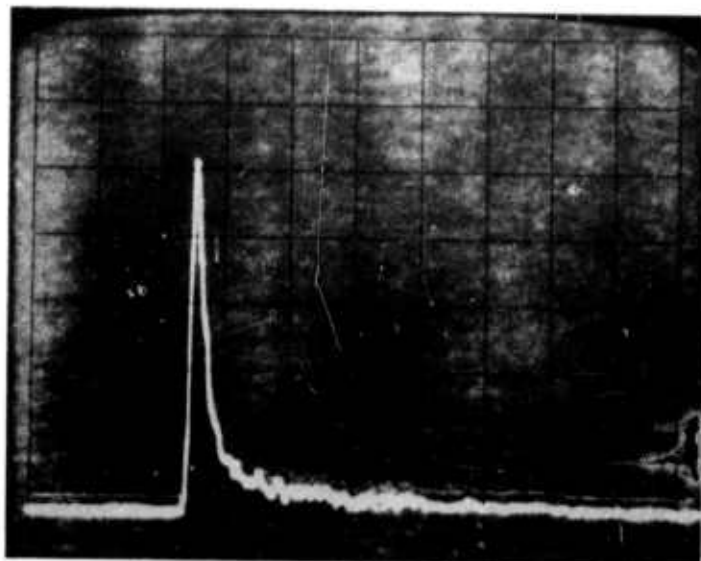


Figure 17

Time evolution of a single pulsed excitation of the 6400Å band in the e-beam afterglow at 3 atmospheres of helium in the HPAC-1 system. Scales are 200 nanoseconds per horizontal division and 270 watts/liter per vertical division. Data shown was obtained with a 1.0 neutral density filter with the scale adjusted accordingly.

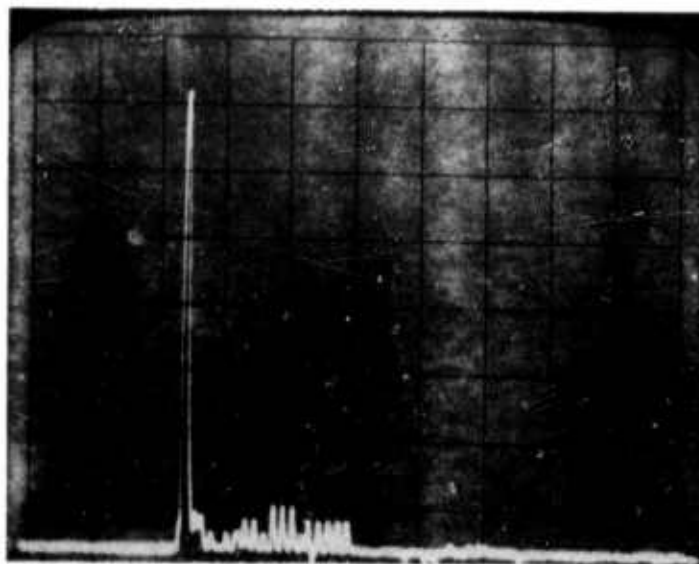


Figure 18 : Time evolution of a single pulsed excitation of the 5015⁰_A line which shows only a component due to direct e-beam excitation. Scales are 200 nanoseconds per horizontal division and 25.6 watts/liter per vertical division.

the most sensitive scale currently available. Only the initial spike temporally mapping the system response to the 3 nanosecond beam excitation is significant. The remainder of the trace is a result of RF1 escaping from the nested enclosures.

A typical example of an emission showing a combination of direct e-beam, and recombination excitation is found in the data of Figure 19. In this figure the emission of the $3^3S \rightarrow 2^3P$ line of atomic helium at 7065\AA is recorded on a horizontal scale of 200 nanoseconds/division by 81 watts/liter per division vertically. While the upper 3^3S state of this transition is optically forbidden to the ground 1^1S state and hence an unlikely candidate for excitation by the primary electrons, it does have a non-zero cross section for secondary electrons which might be expected to have energies near the threshold for excitation of this system. Most probably the situation here is analogous to the excitation of the N_2 C-state in the e-beam N_2 laser. That state is also optically forbidden to the ground X-state and as a consequence is only weakly excited by the higher energy primary electrons but strongly excited by the secondary electrons whose energy lies only slightly above the excitation threshold.

Detailed examination of an expanded time base of the leading edges of the molecular emission as typified by the one at 6400\AA show no evidence of a component of e-beam excitation either by primary or secondary electrons as would be expected from the absence of a stable He_2 ground state. Rather the leading edge shows a rise time consistent with the decay of the component of

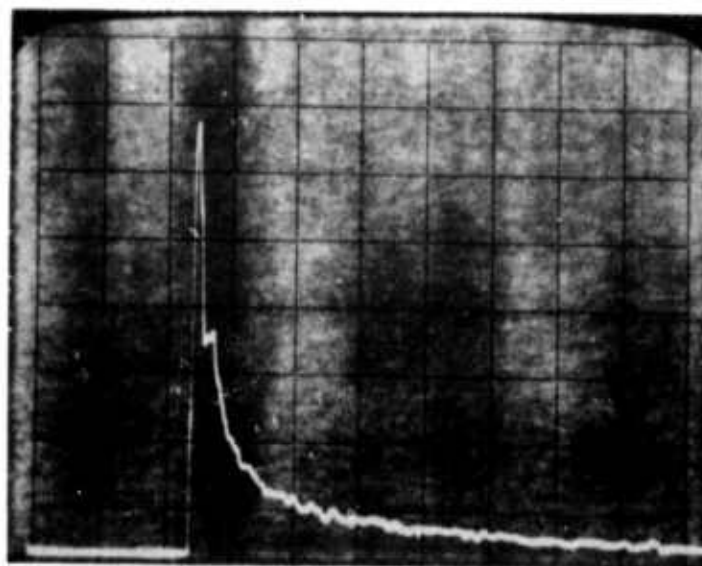


Figure 19: Time evolution of a single pulsed excitation of the 7065⁰ Å line which shows both an early component due to excitation from energetic secondary electrons and a later recombination component. Scales are 200 nanoseconds per horizontal division and 81 watts/liter per vertical division.

the 7065Å excitation inferred to be due to the secondary electrons. This also is consistent with a simple model which requires the secondary electron to cool before they can participate in collisional recombination with the ions. If they are energetic enough to excite the 7065Å line, they are too hot as a group to recombine with the He_2^+ ions to give the 6400Å radiation.

From these considerations and interesting comparison can be made of the output energies resulting from each process. These are summarized in Table III.

Table III
Comparison of Measured Output Energies
from Direct Excitation and Recombination
at 3 Atmospheres

Line	Direct e-beam Excitation (micro-Joules/liter)	Recombination (micro-Joules/liter)
5015Å	~ 1.8	-
7065Å	~16	71
6400Å	< 2.7	110

Table III serves to underscore the comments made in Section II that the potential for recovering much of the e-beam energy "lost" to ionization is quite high in recombination systems.

Implicit in the development of data of the sort presented in Table III is a knowledge of lifetimes by which the peak powers are

are multiplied to estimate the output energy per pulse. The particular lifetimes desired are the lifetimes against recombination defined by equation (7), Section II. In fact, the determination of this lifetime is useful both as a confirmation of the recombination origin of the light and as an effective pulse duration to convert peak power to pulse energy. Such a lifetime can be determined in terms of measured quantities as follows:

Starting from the more general expression for the collisional recombination rate coefficient, equation (5),

$$\alpha = K [e]^n (T_e/300)^{-9/2} \quad , \quad (5)$$

the continuity equation for ion density, neglecting diffusion at these pressures, as well as competing reactions, and assuming $[He_2^+] = [e]$, and a constant $T_e \approx 300^\circ$, then

$$[He_2^+ (t)]^{-(1+n)} - [He_2^+ (0)]^{-(1+n)} = (1+n)Kt \quad . \quad (14)$$

Now it is expected⁹ that the photon emission rate in any particular band during the course of the stabilization of the recombination should approximately equal some constant fraction, f , of the recombination rate of the ions, which allowing for geometric collection factors and sensitivities implies that

$$I(t) = C K [He_2^+ (t)]^{2+n} \quad , \quad (15)$$

where C represents all collected scale factors. Substituting (15) into (14) gives:

$$\frac{I(t)^{-\frac{1+n}{2+n}} - I(0)^{-\frac{1+n}{2+n}}}{t} = (1+n)(CK)^{-\frac{1+n}{2+n}} K \quad . \quad (16)$$

This implies that a plot of intensity to the $-(1+\eta)/(2+\eta)$ power would be a linear function of time and that the slope, S , of such a curve would be simply the right-hand side of (16). Defining then

$$S = (1+\eta)(CK)^{-\frac{1+\eta}{2+\eta}} K \quad (17)$$

enables the effective lifetime of the collisional recombination defined by equation (7) to be written in terms of experimentally measured parameters as

$$\tau_0^{-1} = \alpha[\text{He}_2^+(0)] = S(1+\eta)^{-1} I_0^{\frac{1+\eta}{2+\eta}} \quad (18)$$

Examination of this equation in comparison with (17) shows τ_0^{-1} to be independent of the scaling of the intensity as would be expected.

Finally considering the energy per pulse E , this can be expressed

$$E = \int_0^\infty I(t) dt \quad , \quad (19)$$

which becomes upon substitution from (16)

$$E = \int_0^\infty \left\{ I(0)^{-\frac{1+\eta}{2+\eta}} + K(1+\eta)(CK)^{-\frac{1+\eta}{2+\eta}} t^{\frac{2+\eta}{1+\eta}} \right\} dt \quad (20)$$

Upon integration followed by substitution from (18) and (17), this becomes

$$E = I(0)\tau_0 \quad (21)$$

These results suggest the procedure of plotting the inverse intensity to the $(1+\eta)/(2+\eta)$ power for various trial values of η between 0 and 1, determining the best straight line slope, if any,

and then obtaining the recombination lifetime from (18).

Equivalent pulse energies can then be found from (21).

Figure 20 shows the 6400Å decay in the HPAC-1 system at 3 atmospheres pressure to the highest useful time resolution, 40 nanoseconds per division, and Figures 21, a through d show the resulting plots of I^{-M} for four trial values for M, .50, .55, .60, and .66 corresponding to values of η equal to .0, 0.22, 0.5, and 1.0, respectively.

Although there is no unequivocal choice between the four, it appears that $\eta = 1$ could be preferred because of the longer range of linearity realized. In that case, the lifetime would be 79 nanoseconds.

In the latter stages of the reporting period lifetime measurements were greatly facilitated in both speed and accuracy by interfacing the Biomation 8100 transient recorder to the on-line data acquisition computer serving the University's Atomic Physics group. A digital image of each decay curve could be stored and the required inverse intensity plots to the various fractional powers plotted. Data for the three principal spectral features at 6400Å, 5875Å, and 4650Å for afterglows at the three pressures, 1, 3, and 4.2 atmospheres in the HPAC-1b system are shown in Figures 22 through 24, together with the resulting computer analyses and plots.

Lifetimes of the two molecular features, 6400Å and 4650Å show reasonable agreement over the range of pressures examined

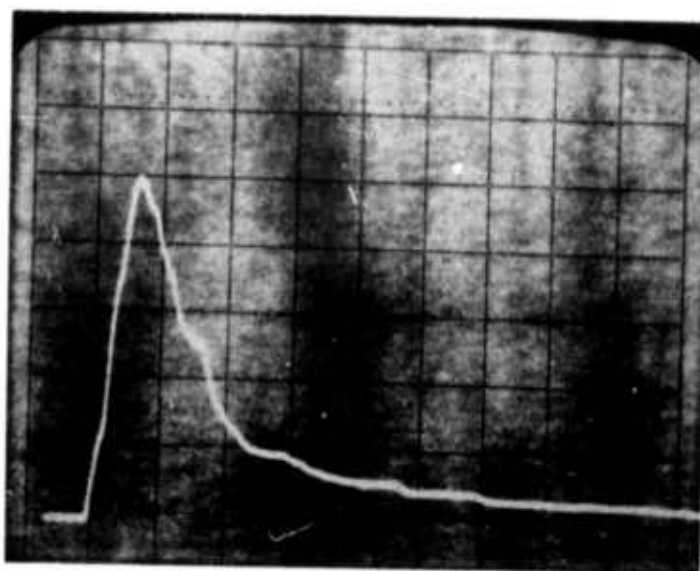
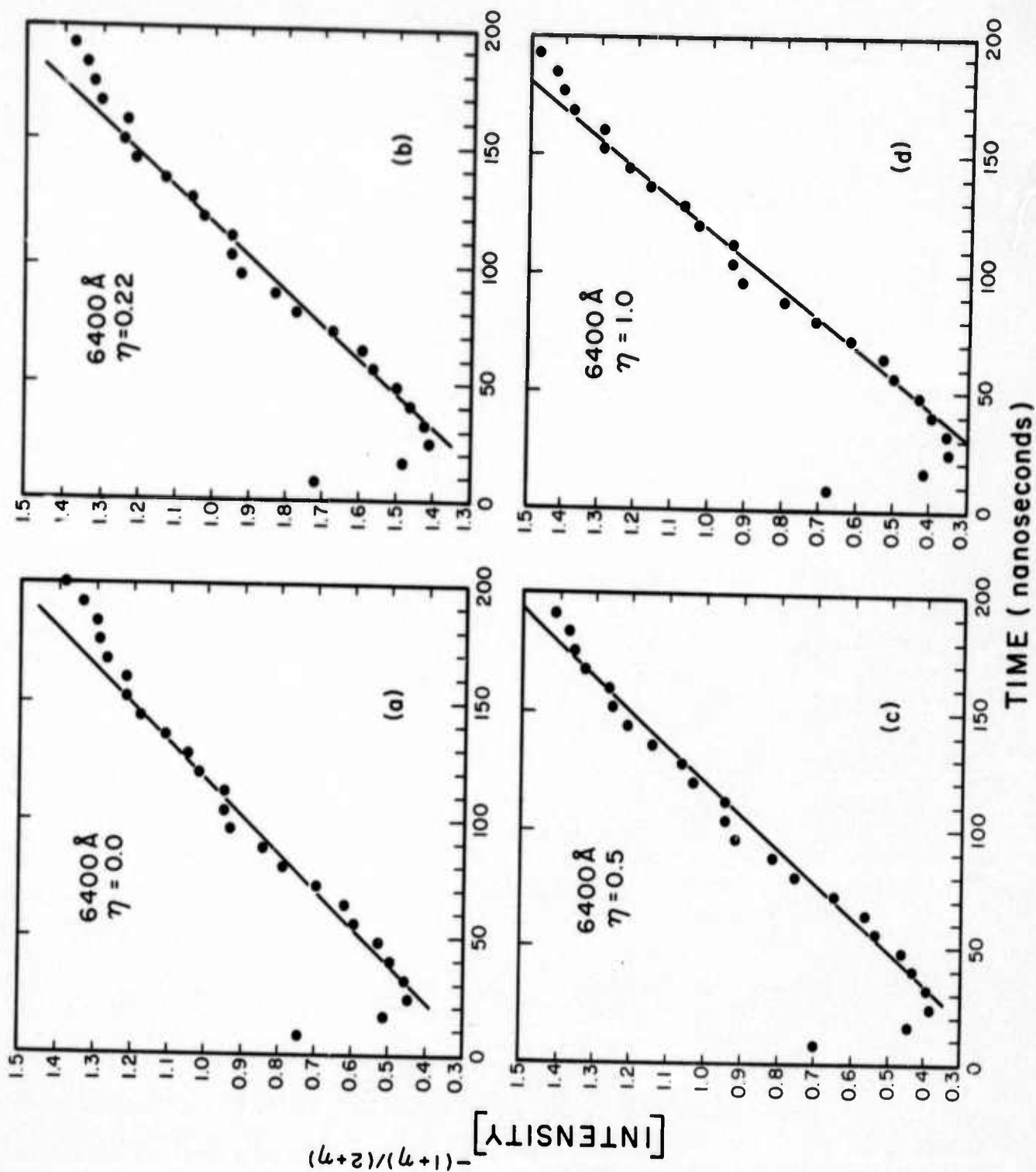


Figure 20: Time evolution of the 6400\AA band of recombination origin shown to the highest useable time resolution, 40 nanoseconds per horizontal division.

Figures 21

Plots of inverse intensity to the M-power as functions of decay time for four models of collisionally-stabilized recombination.

- a) $\eta=0$; pure neutral stabilization
- b) $\eta=0.22$
- c) $\eta=0.5$
- d) $\eta=1.0$; pure electron stabilization



Figures 22

Three data plots showing the time evolution and its analyses of the 6400Å emission in the afterglow from single discharges of the e-beam, sequentially at 1,3, and 4.2 atmospheres pressure in the HPAC-1b system.

Each page shows, counterclockwise from the upper left,

- a) Photograph of the refreshed oscilloscope trace of the analog reconstruction of the stored transient.
- b) Plot of the digital image of the stored transient.
- c) Plot of the inverse intensity to the M-power as a function of decay time for $\eta=0$, neutrally stabilized recombination.
- d) Plot of the inverse intensity to the M-power as a function of decay time for $\eta=1$, electronically stabilized recombination.

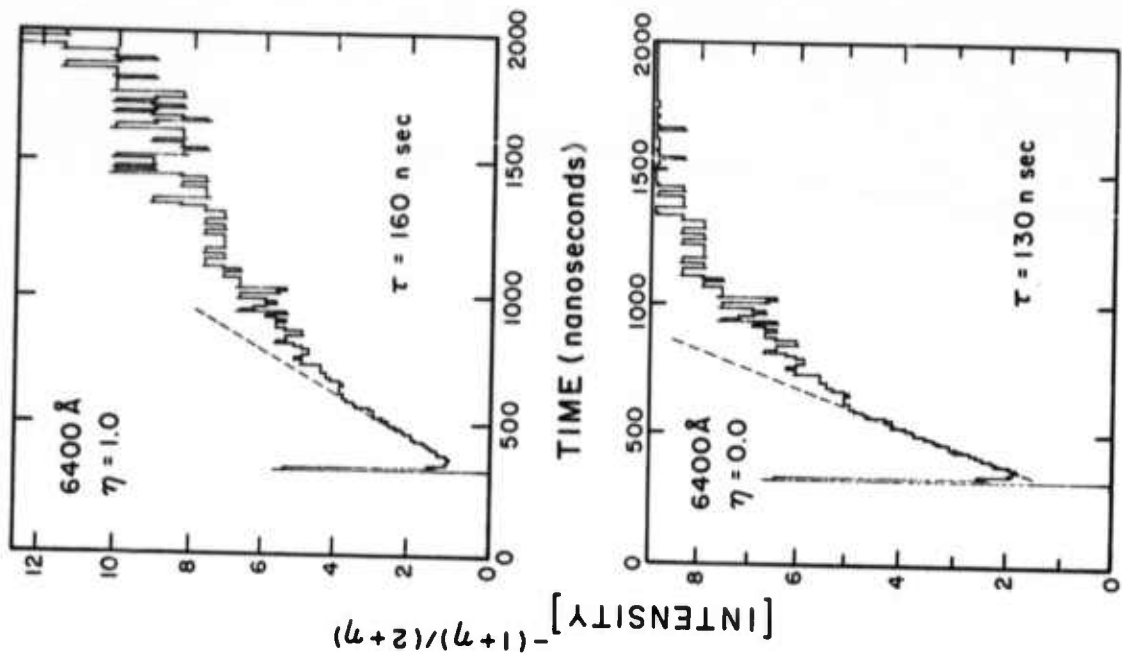
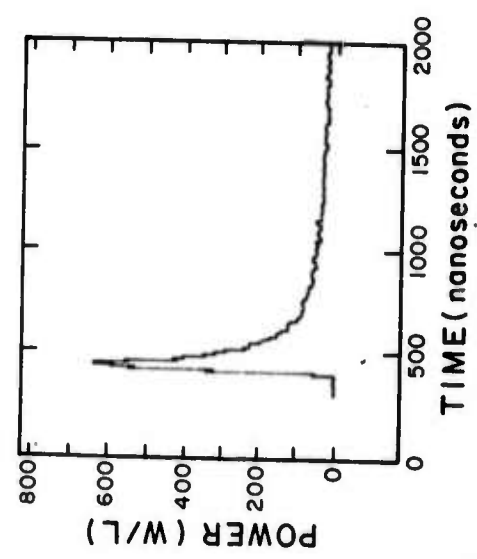


Figure 22 a

Scale: 40 nanoseconds per horizontal division
0.05 Volts per vertical division



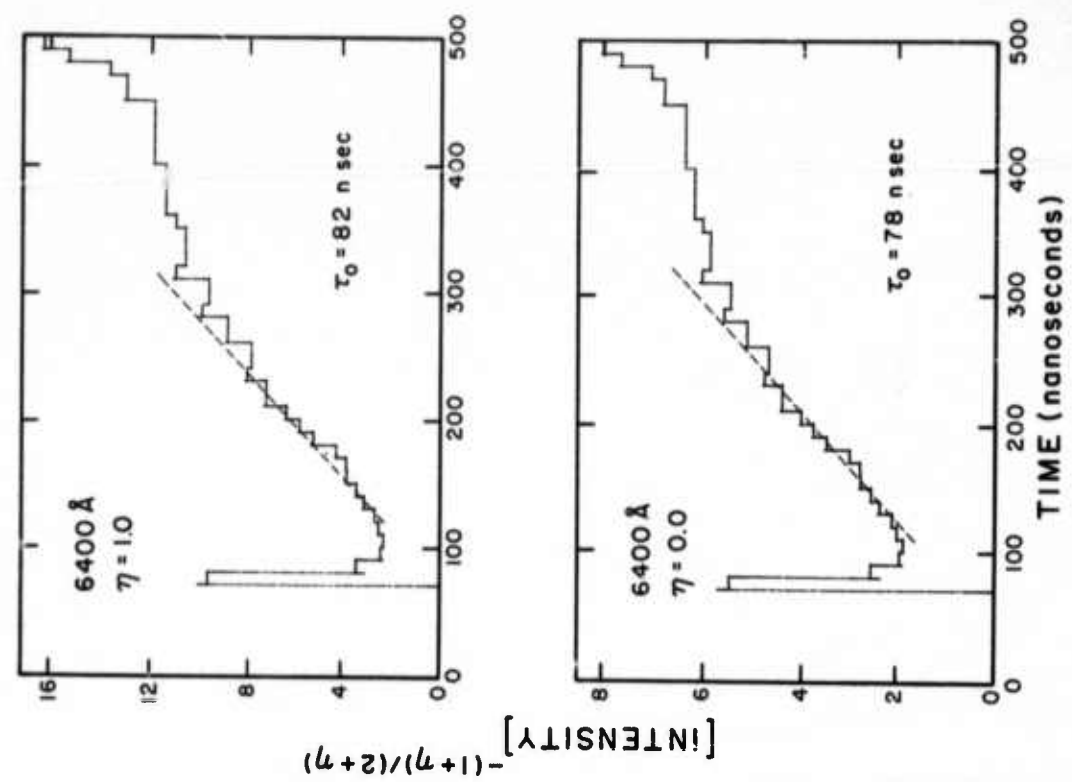
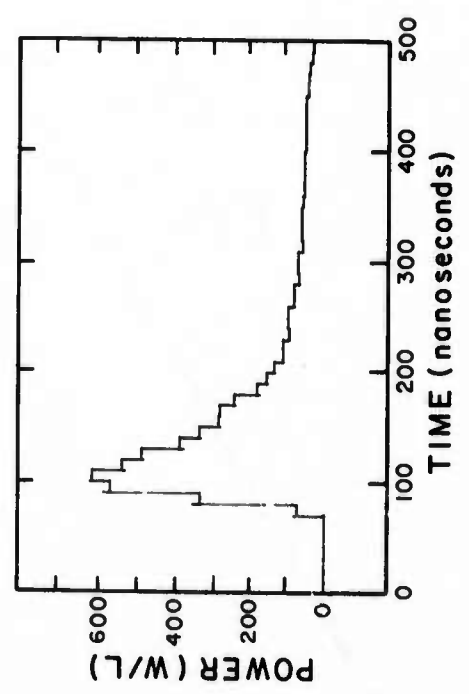


Figure 22 b



Scale: 40 nanoseconds per horizontal division
0.05 Volts per vertical division



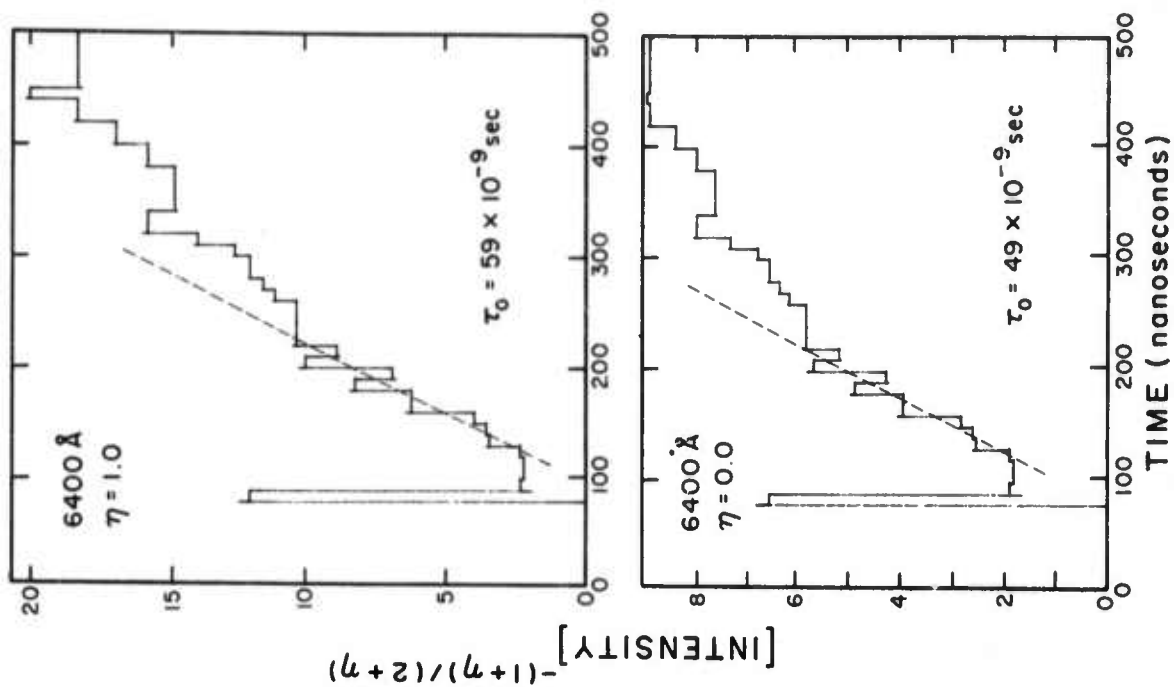
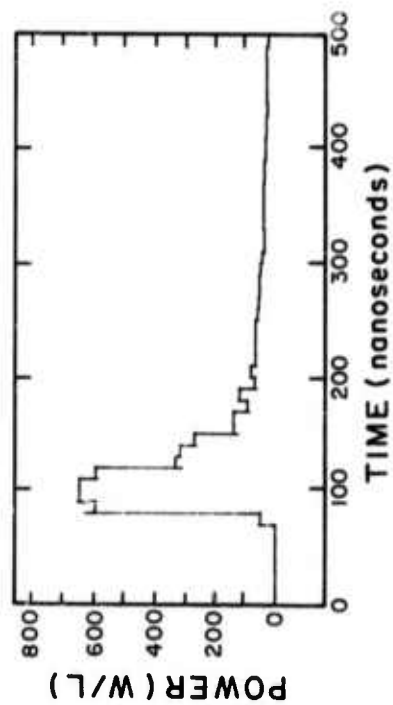


Figure 22 c



Scale: 200 nanoseconds per horizontal division
0.05 Volts per vertical division



Figures 23

Three data plots showing the time evolution and its analyses of the 5875\AA emission in the afterglow from a single discharge of the e-beam, sequentially at 1, 3, and 4.2 atmospheres pressure in the HPAC-1b system. Each page shows, counterclockwise from the upper left,

- a) Photograph of the refreshed oscilloscope trace of the analog reconstruction of the stored transient.
- b) Plot of the digital image of the stored transient.
- c) Plot of the inverse intensity to the M-power as a function of decay time for $\eta=0$, neutrally stabilized recombination.
- d) Plot of the inverse intensity to the M-power as a function of decay time for $\eta=1$, electronically stabilized recombination.

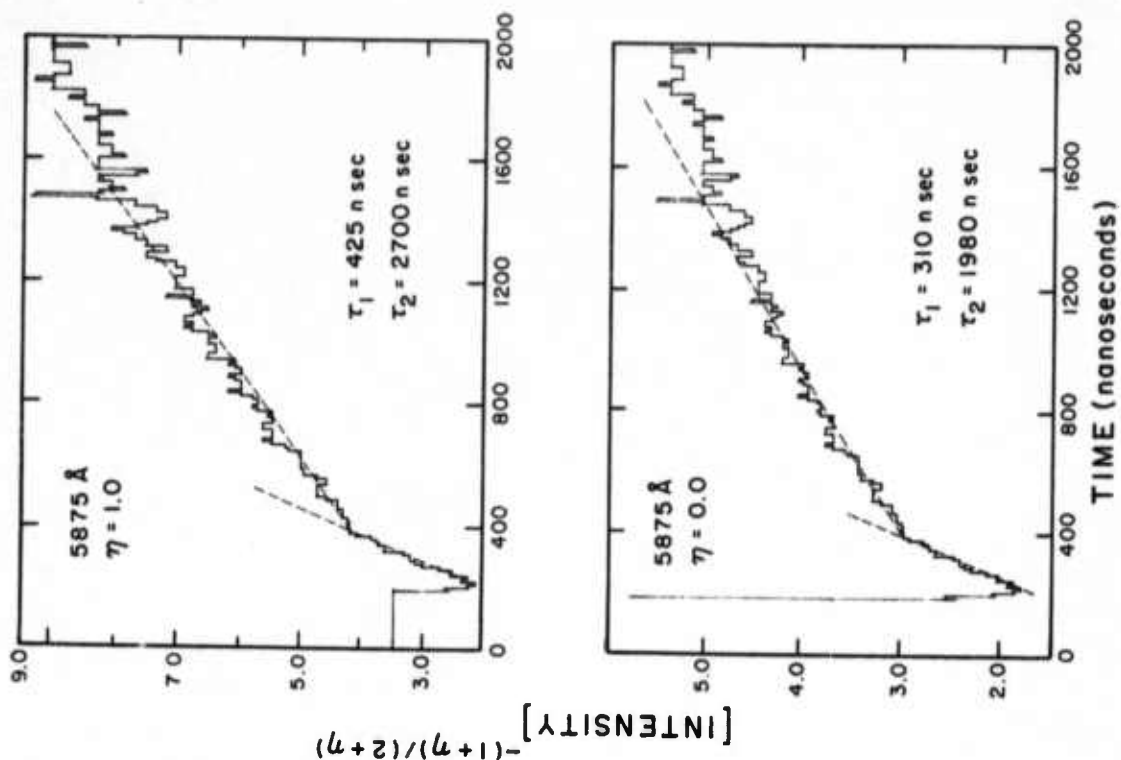
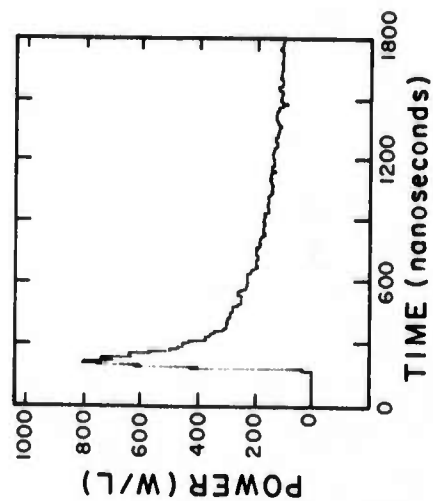


Figure 23 a



Scale: 200 nanoseconds per horizontal division
0.05 Volts per vertical division



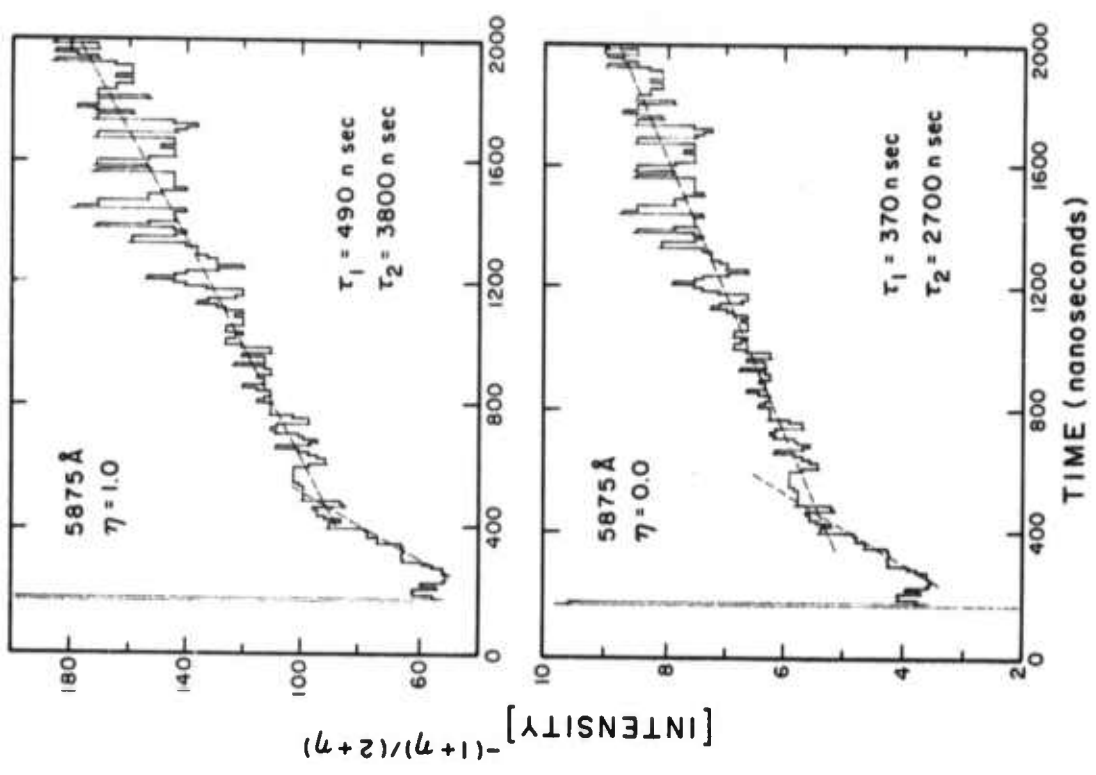
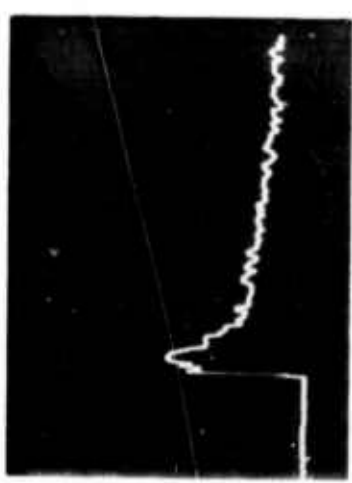


Figure 23 b



Scale: 200 nanoseconds per horizontal division
0.025 Volts per vertical division

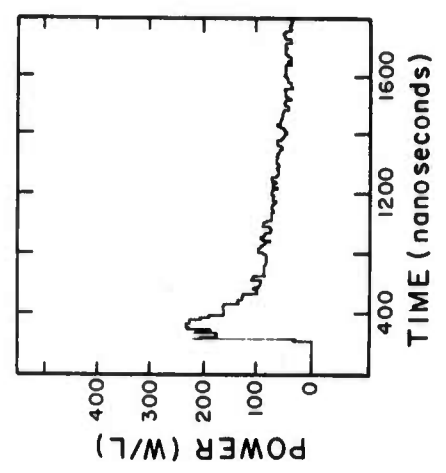
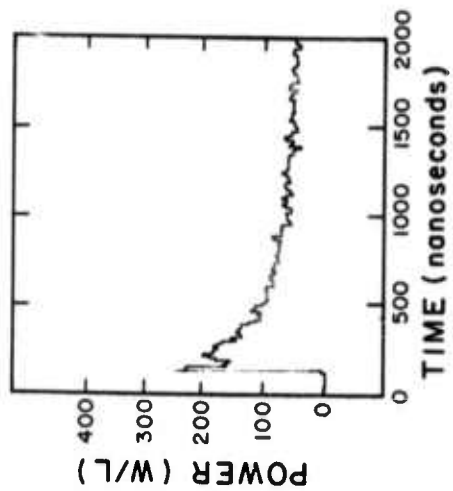


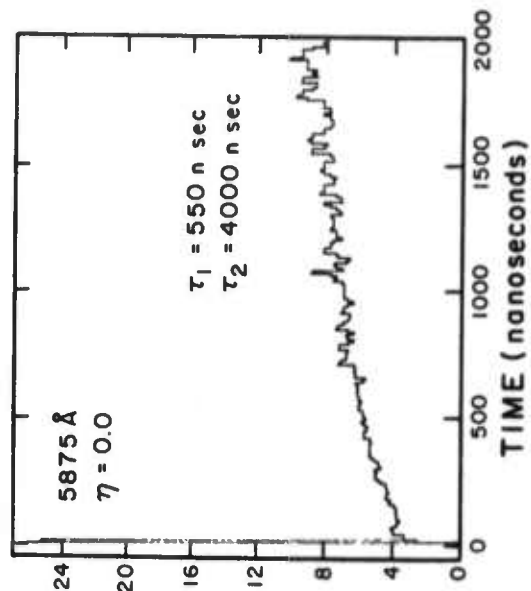
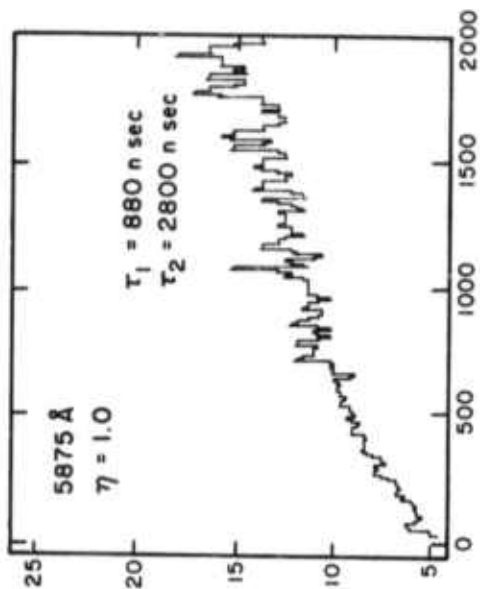
Figure 23 c



Scale: 200 nanoseconds per horizontal division
0.025 Volts per vertical division



[INTENSITY]
 $-(1+\eta)/(2+\eta)$



Figures 24

Three data plots showing the time evolution and its analyses of the 4650\AA emission in the afterglow from a single discharge of the e-beam, sequentially at 1, 3, and 4.2 atmospheres pressure in the HEAC-1b system. Each page shows, counterclockwise from the upper left,

- a) Photograph of the refreshed oscilloscope trace of the analog reconstruction of the stored transient.
- b) Plot of the digital image of the stored transient.
- c) Plot of the inverse intensity to the M-power as a function of decay time for $\eta=0$, neutrally stabilized recombination.
- d) Plot of the inverse intensity to the M-power as a function of decay time for $\eta=1$, electronically stabilized recombination.

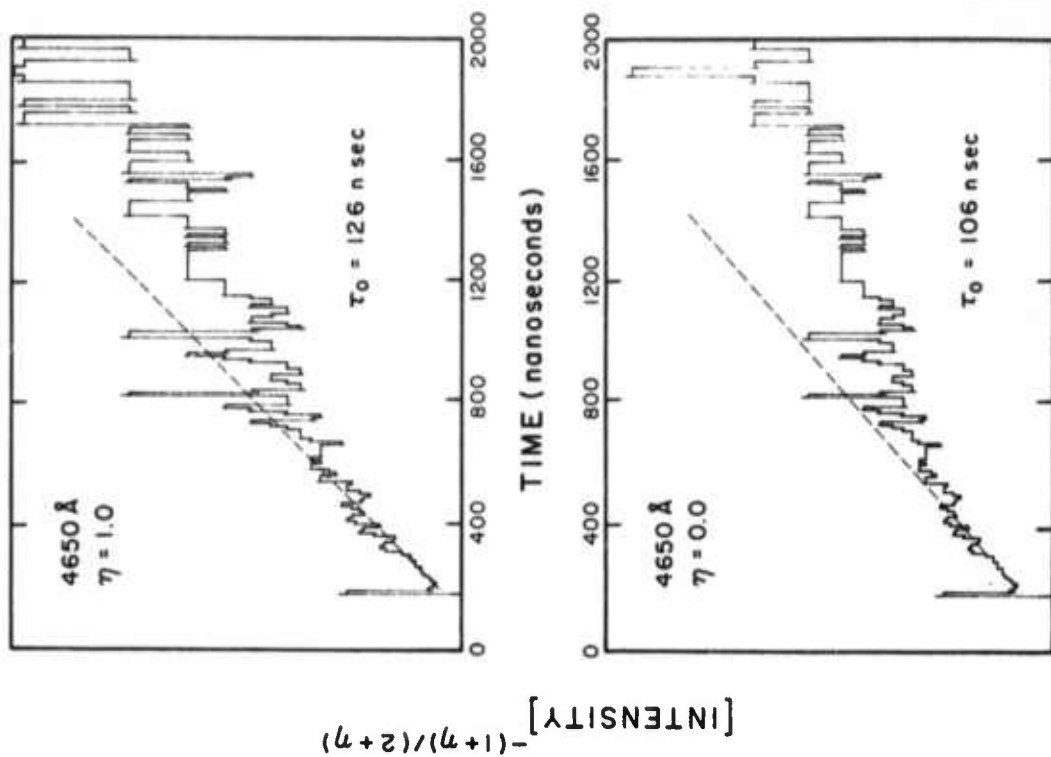
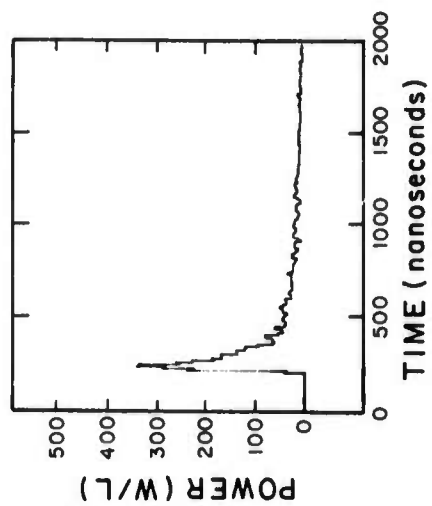


Figure 24 a



Scale: 200 nanoseconds per horizontal division
0.025 Volts per vertical division



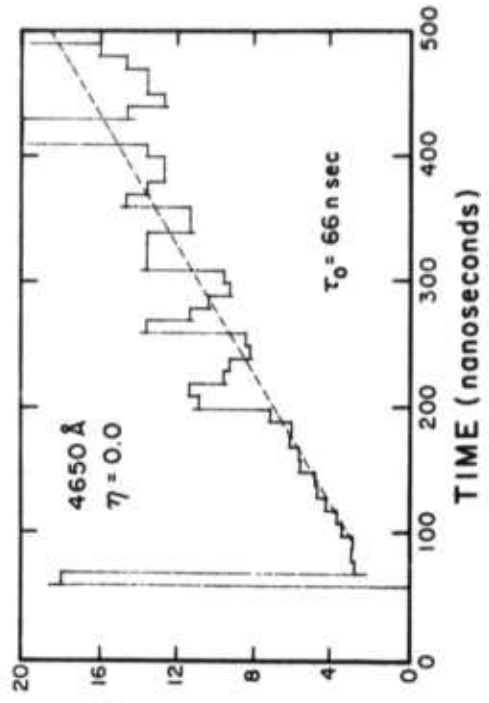
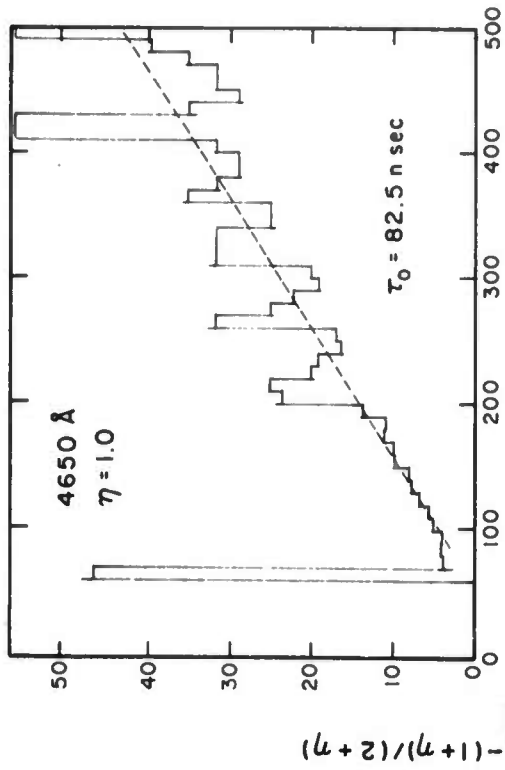


Figure 24 b



Scale: 40 nanoseconds per horizontal division
0.025 Volts per vertical division

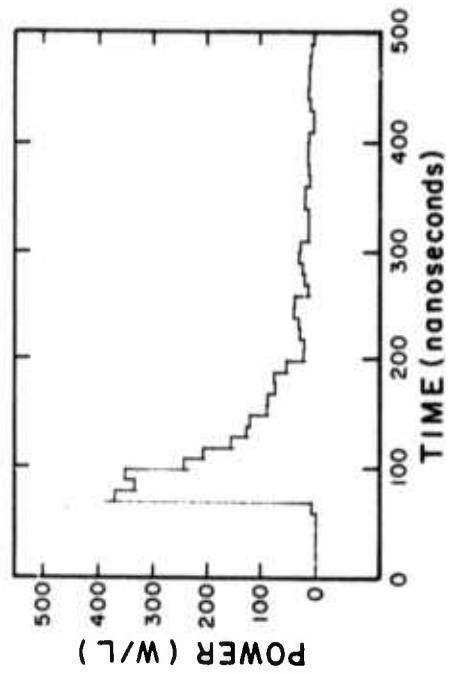
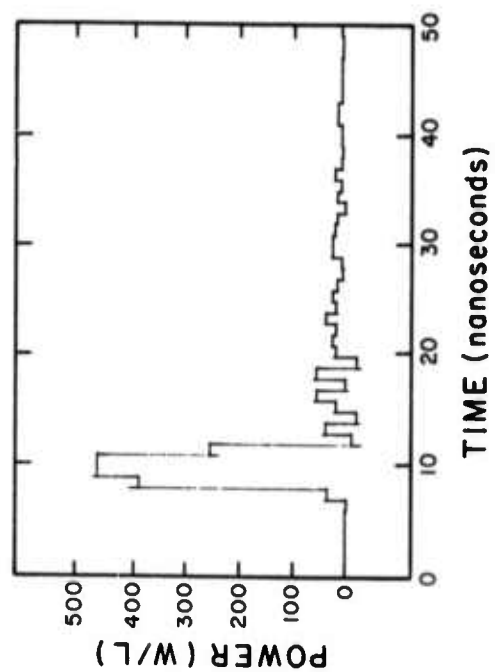


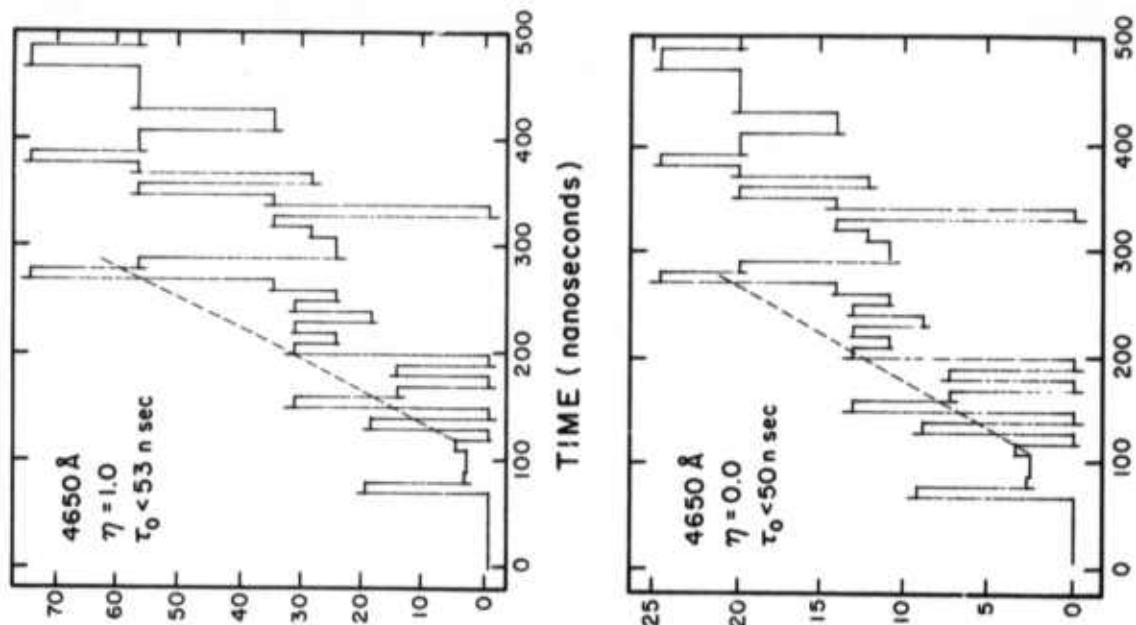
Figure 24 c



Scale: 40 nanoseconds per horizontal division
0.025 Volts per vertical division



[INTENSITY]
 $-(1+\eta)/(2+\eta)$



and suggests the validity of the assumption summarized in equation (15) that the emitted intensity is a constant fraction of the energy released by the recombining He_2^+ ions.

The converse behavior was found for the recombination portion of the decay of the atomic lines examined. Lifetimes deduced did not agree with the recombination rates for the molecular bands or even with each other. The most extreme divergence was shown by the $3^3\text{D} \rightarrow 2^3\text{P}$ transition at 5875\AA which is reproduced in Figures 23

The lifetime is anomalously long as can be seen upon inspection, and consists of two slopes as shown in the corresponding analyses which present the inverse intensities for various η . Other atomic lines did not show the two lifetime behaviors but did show scattered lifetimes. Results for lifetimes and pulse energies are collected in Table IV.

The rather extreme variation of atomic recombination lifetimes strongly indicates that for the production of excited atoms the assumption expressed by (15) does not hold and that the relative importance of the various stabilizing channels is a changing function of electron density and hence, time. This is in general agreement with the results of 0.1 atmosphere work which has demonstrated that the molecular bands tend to have the same time decays¹⁰ in agreement with (15) while the atomic lines do not⁹.

Table IV

Summary of Lifetimes and Incoherent Energies
per Pulse of the Principal Spectral Features

Wavelength	Lifetime $\eta=1$ (nanoseconds)				Energy (micro-Joules/liter)			
	1	3	4.2	-7	1	3	4.2	7
<u>He₂</u>								
6400Å	160	82	59	26*	104	52.5	35.0	32*
4650Å	126	82.5	53	34*	42.5	31.4	25.2	24*
<u>He</u>								
7065Å	-	267	350*	93*	-	54*	59*	92*
6678Å	208*	100*	45*	29*	38.6*	24.2	12.1*	15.0*
5875Å early	880	490	425	300*				
late	2800	3800	2700	2320*	665	905	2200	4400*
* HPAC-2 system								

- c) Incoherent output efficiencies -- From the data of Table IV and the input e-beam energy estimated in equation (11), the output efficiency can be obtained for the prominent spectral features examined. Table V summarizes these results.

Table V

Efficiencies for the Incoherent Radiation
Observed from the Recombination

Wavelength Pressure (atm)	Efficiency		
	1	3	4.2
<u>He₂</u>			
6400Å	.0057%	.00096%	.00054%
4650Å	.0023%	.00057%	.00032%
<u>He</u>			
7065Å	--	.001%	.001%
6678Å	.002%	.0004%	.00015%
5875Å	.036%	.016%	.028%

Efficiencies are not particularly impressive but this is not surprising because in the absence of a stimulated transition, at these electron densities a large fraction of the level to level stabilization should be accomplished by non-radiative transitions. According to theory, if a stimulated transition can be developed the energy now lost to the collisional channels could be tapped by a competing radiative transition, if strongly induced.

- d) Inferred optical gains -- The gain or loss of selected transitions was inferred basically from the measurement of the relative enhancement of the feature observed in a resonant optical cavity.

Interpretation of such data is difficult at best, but in the present case it was greatly facilitated by the results of a concurrent project at this institution. A very intensive study has recently been completed by Blanaru¹⁵ on the estimation of gain and loss in resonant optical cavities lying between confocal and concentric geometries. Extensive calibrations have been made of such cavities with helium-neon lasers to verify the interpretive model to $\pm 1\%$ gain per cavity transit. Within these limits it is believed warranted to use the interpretative models which consisted of numerically integrated extensions of the early Ladenburg-Reiche method¹⁶.

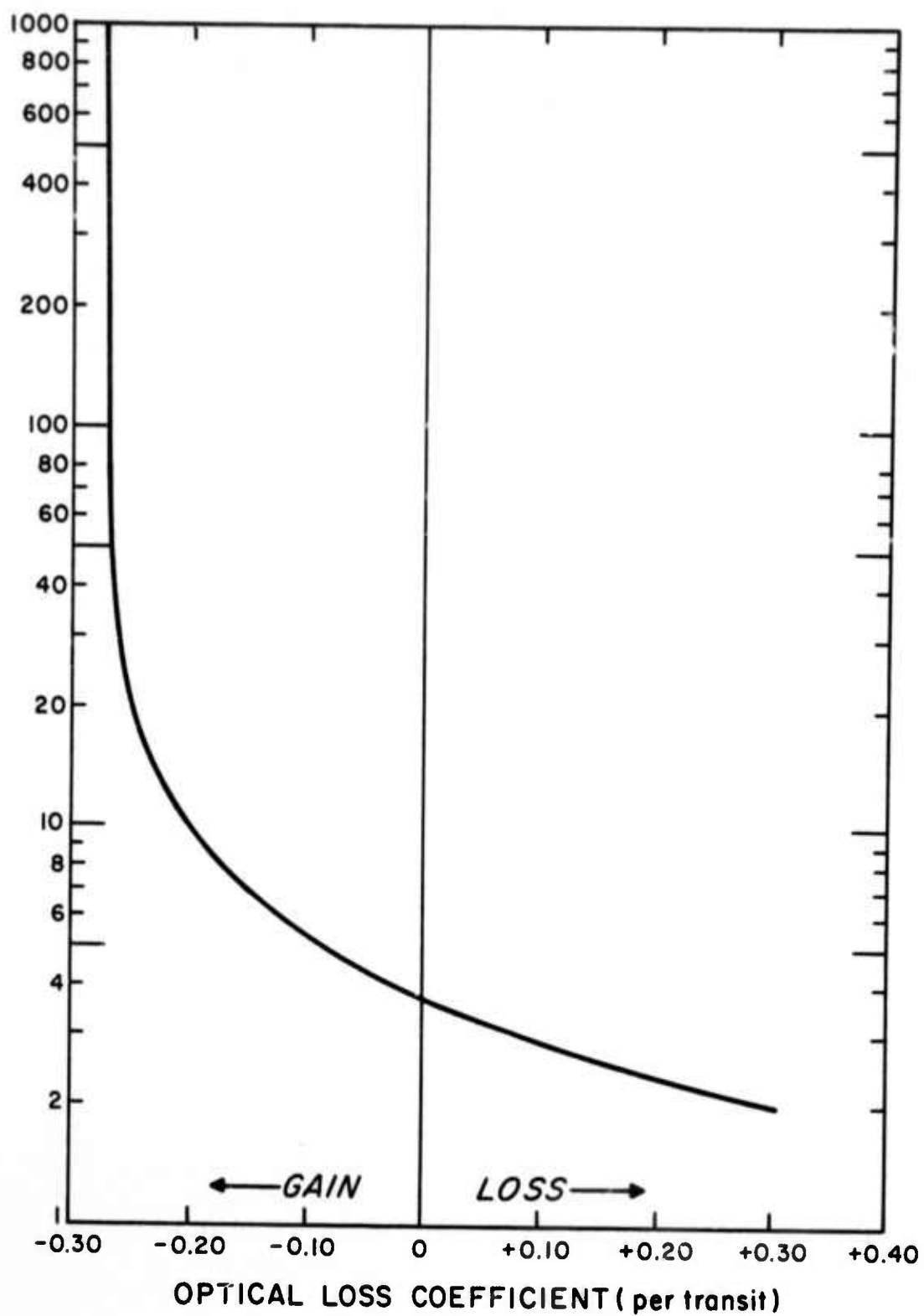
The primary cavity parameter which must be determined to scale the measurement is a geometric efficiency, G , which essentially relates the total plasma volume sampled to the volume interacting with the cavity. It is a function of cavity length, mirror diameter and the axial distance to the point of observation. The principal system parameter is the passive optical transmissivity, a_0 , of the afterglow container and cavity per roundtrip transit of the cavity. Assuming then a Doppler-broadened profile in a non-oscillating cavity the model shown in Figure 25 was calculated for the measured value of $a_0 = 0.58$ characteristic of the system with normal incidence quartz windows in HPAC-1. The fractional gain (negative) or loss (positive) values per transit of the medium are plotted as abscissas. Ordinates give the corresponding value of

$$F = G(M-1) \quad , \quad (22)$$

Figure 25

Plot of calculated F-factor from equation (22) as a function of fractional loss (+) or gain (-) coefficient per transit of the plasma. The value of passive optical transmissivity corresponding to the measured 0.58 has been used in the computational model.

q'

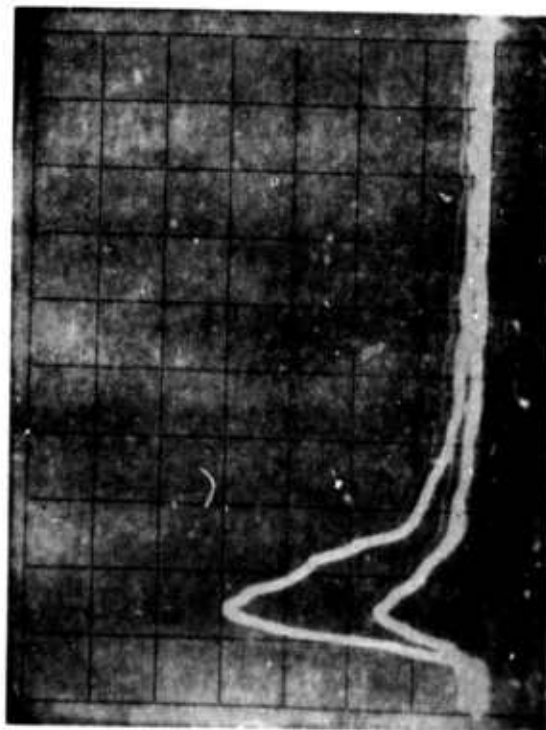


where M is the enhancement ratio of intensity sampled from the cavity to the intensity sampled by the same system with the mirror farthest from the point of observation covered. In the case of the measurement to be discussed below the geometric factor G was calculated to be 4.85.

The particular concave mirrors used in the cavity were multi-layer dielectrics selected to give maximum reflection over the range 6000 to 6800 Å. However, calibration showed mirror losses to be less than 0.5% at 5875 Å and 7065 Å so that the transmissivity coefficient would be perturbed less than ± 0.01 by the extension of the measurements to include these two lines.

Light from the cavity was sampled from observation of the reflection from a thin plate interposed in the cavity and inclined 45° to the optical axis. Since the loss to the cavity contributed by the sample plate has been included in the transmissivity factor a_0 , it can be seen that intensities reaching the detector will be down more than an order of magnitude. In fact, it was necessary to remove both slits from the 0.25m. spectrometer in order to obtain useable signal to noise ratios. Consequently, spectral resolution was reduced to 120 Å. Nevertheless, this proved sufficient to isolate the principal features examined.

Figures 26 a and b show the enhancement obtained in the cavity at 6400 Å and 6678 Å, respectively. Horizontal scale is 40 nanoseconds/division. Reproduceability was of the order of 0.1 division. The difference in degree of enhancement is quite marked. The characteristic values of M at the curve peaks are 2.6 and 1.9 for 6400 and 6678, respectively. From (22) the ordinate, F for Figure 25 becomes 7.8 and 4.4, respectively, and correspond to a gain of 17% per transit in the first case and a gain of 5% in the second.



a) He_2 band at 6400\AA



b) He line at 6678\AA

Figures 26: Time-resolved enhancements of intensity observed in the resonant near-confocal cavity during single e-beam excitations at 3 atmospheres of helium. In each the upper curve is the enhanced intensity and the lower, the normal afterglow emission. Horizontal scale is 40 nanoseconds/division.

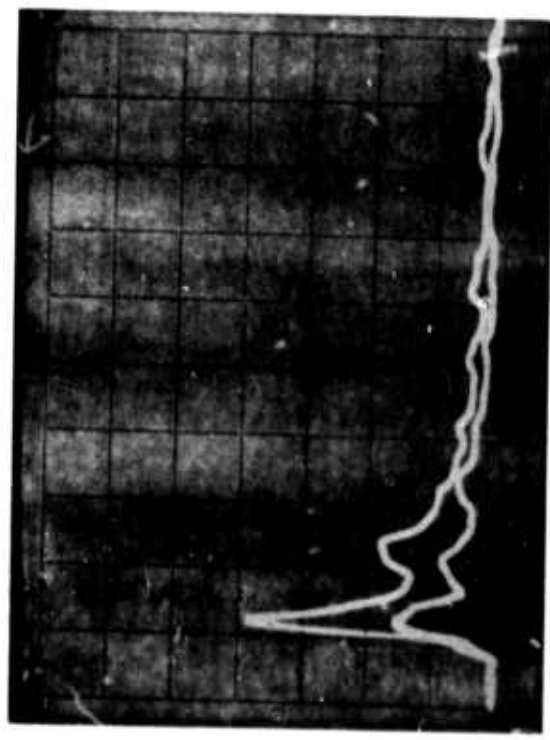
However, the statistical uncertainty of ± 0.1 division in both elements of the ratio M for 6678\AA , when combined according to standard statistical procedures, serve to introduce a probable error of ± 0.2 in M and a consequence uncertainty in F bounding it by 6.8 and 8.7. From Figure 25, this implies a value of gain per transit lying between 15 and 19% and having a nominal value of 17%.

Records of the remaining features in the region at 7065\AA and 5875\AA are shown in Figures 27a and b. In these cases signal was quite low and noise a very serious problem. The 7065\AA data is interesting in that it shows a reproducible enhancement of about $M = 2.5$ in the direct excitation spike on the leading edge and $M \leq 2.0$ in the afterglow tail. The difference is between an implied 16% gain per transit and a nominal 8% gain.

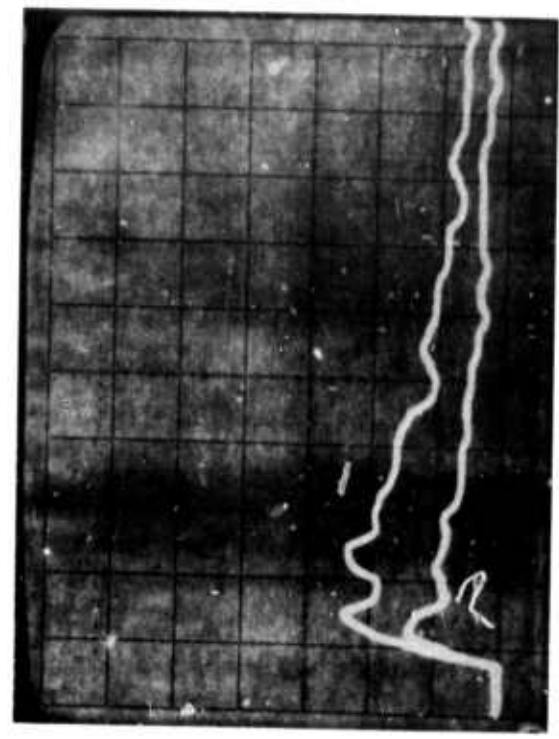
Analysis of the 5875\AA data is defeated by the noise although some evidence can be inferred for a change from small loss to small gain as the decay proceeds.

Figure 28 shows the enhancement of the 4650\AA band in the same optical geometry as the red data just presented, but with the mirrors replaced with a concave pair having maximum reflectivity spanning the range 3950 to 4700\AA . Absorption could be expected for this transition due to the metastability of the lower $2s^3\Sigma_u^+$ state. This was, in fact, observed at the peak, the ratio M from Figure 28 being 1.46 and the consequent F , 2.23. This is beyond the range of validity of the model presented in Figure 25 but extrapolative indications imply an absorption coefficient of 0.23 per transit, which is a loss in excess of 23%.

The results of these measurements are summarized in Table VI.



a) He line at 7065\AA



b) He line at 5875\AA

Figures 27: Time-resolved enhancements of intensity observed in the resonant near-confocal cavity during single e-beam excitations at 3 atmospheres of helium. Horizontal scale is 40 nanoseconds/division.

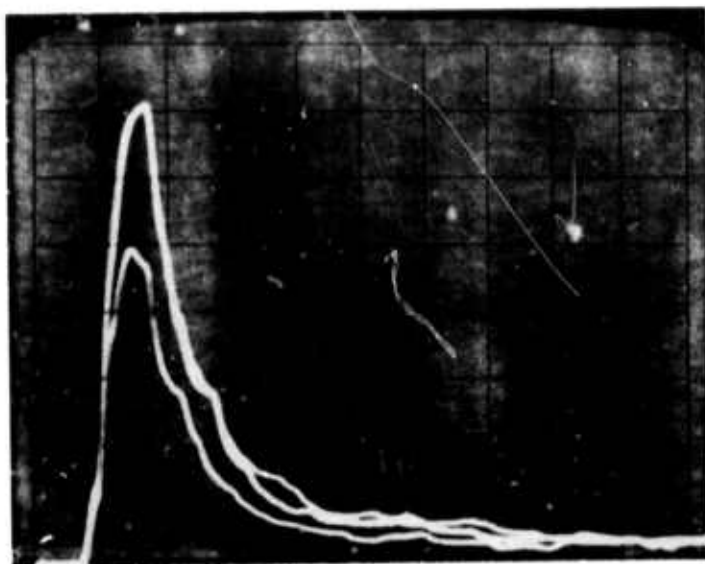


Figure 28 : Time-resolved enhancement of intensity of the absorptive 4650^oÅ band of He₂ observed in the near-confocal cavity during single e-beam excitations at 3 atmospheres of helium. Horizontal scale is 40 nanoseconds/division.

Table VI

Optical Gains per Cavity Transit
Inferred from Measurement

Wavelength	Cavity Enhancement Ratio, M	Coefficient Gain(Loss) per transit
7065Å	~2.5, early	~0.16
6678Å	1.9	0.05
6400Å	2.6	0.17
5875Å	~2.0	0.08
4650Å	~1.46	~(0.23)

Considering the severe signal-to-noise problem in the case of the first and fourth entry, only the measurements at 6678Å and 6400Å should be considered indicative. However, since the plasma length is only about 5 cm along the optical axis, the indicated gain of 17% for 6400Å is quite substantial and consequently of considerable importance. Of course such inferences are very dependent upon the accuracy of the rather complex interpretative model and in view of the high loss per transit of the cavity represent measurements quite far from the lasing threshold.

HPAC-1b represented an attempt to reduce window losses by sealing quartz Brewster-angle windows across the optical axis. Unfortunately the windows were distorted by the sealing process and although the reflective and absorptive losses were quite low, refractive losses from individual rays were quite high and difficult to estimate quantitatively due to the small scale, randomly oriented nature of the distortions.

Figure 29 shows a schematic representation of the system used to investigate enhancement ratios with the HPAC-1b cell. The introduction of Brewster angle windows introduces a loss coefficient which is a function of polarization angle and a sampling efficiency which is also a function of polarization angle.

Since the afterglow is radiating incoherently, all polarizations appear in the sampled beam with some corresponding to lower loss modes than others. The portion of the beam split off to the spectrometer is a linear combination of the components of these various loss modes weighted in intensity by the selectivity of the inclined plate to the different polarizations. For example when the sample plate is at the Brewster angle none of the light of the lowest-loss mode of the cavity is split into the output beam. As a consequence the relative enhancements measured will contain no component of the mode showing the highest ratio. Rotation of the sample plate (angle θ in Figure 29) from the Brewster angle increases the fraction of the high-ratio polarizations sampled, but decreases the enhancement ratio of all modes by introducing additional reflective loss into the cavity for most polarizations.

Some selection for the higher-ratio polarizations can be accomplished by adjusting the angle ϕ of the analyzing polarizer shown in Figure 29. Nevertheless the sampling arrangement was sufficiently complex that quantitative analysis was deemed inconsistent with the actual quality of the Brewster windows. Rather the qualitative aspects were examined in an attempt to determine if the optimistic predictions of gain obtained from HPAC-1 could be supported.

Figure 29

Schematic representation of the optical system used to determine the signal enhancement produced by enclosing the afterglow within a resonant optical cavity.

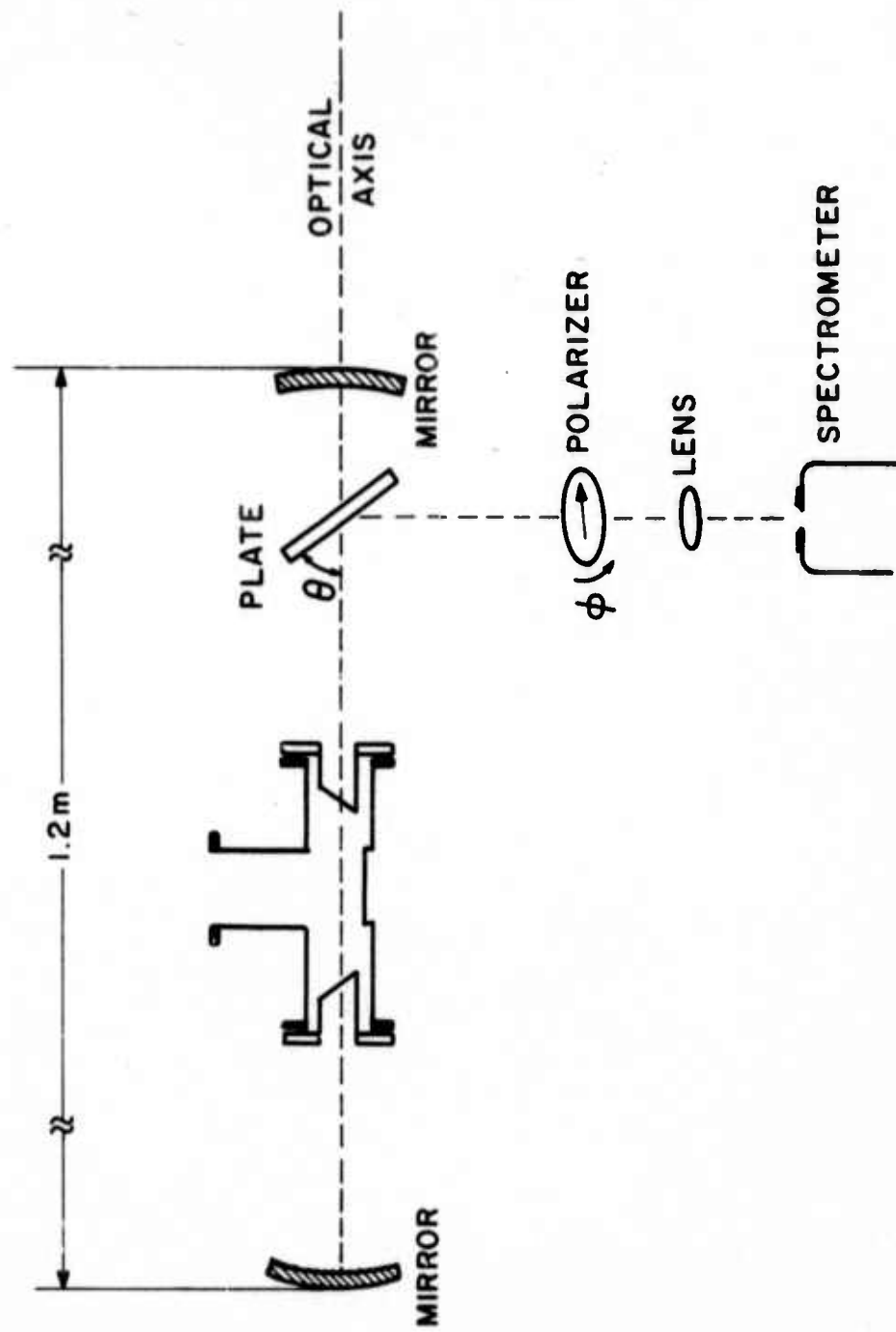


Figure 30 shows the resulting enhancement ratio for the 6400 Å feature at 3 atmospheres pressure in the HPAC-1b system as a function of polarization angle, ϕ for three different angles, θ of the same plate. As can be seen for increasing but small inclinations of the plate to the Brewster angle the peak enhancement is increased in agreement with theoretical expectations. Peak values remain consistent with the magnitude of the gain per transit indicated by the measurements in HPAC-1 discussed in the immediately preceding material.

A much less equivocal indication of gain can be obtained by examining the cavity enhancement ratio as a function of the number of upper state molecules radiating. Referring again to Figure 25, it can be seen that since the abscissa is proportional to product of the population of the upper state and to one minus the inversion ratio, unless the inversion ratio closely approximated unity, a large decrease in excited state population should tend to bring the value of abscissa closer to the coordinate origin. Had the transition been absorptive, the enhancement ratio would increase and had it shown gain the ratio would decrease.

Figure 30

Cavity enhancement ratios for the 6400 \AA emission at 3 atmospheres pressure as functions of polarization angle, ϕ , for the different values of inclination of the sampling plate to the Brewster angle. For the curves peaking from rightmost to the left, $\theta=0$, Brewster angle; $\theta = 1^{\circ}48'$ to the Brewster angle; and $\theta = 3^{\circ}36'$ to the Brewster angle, respectively.

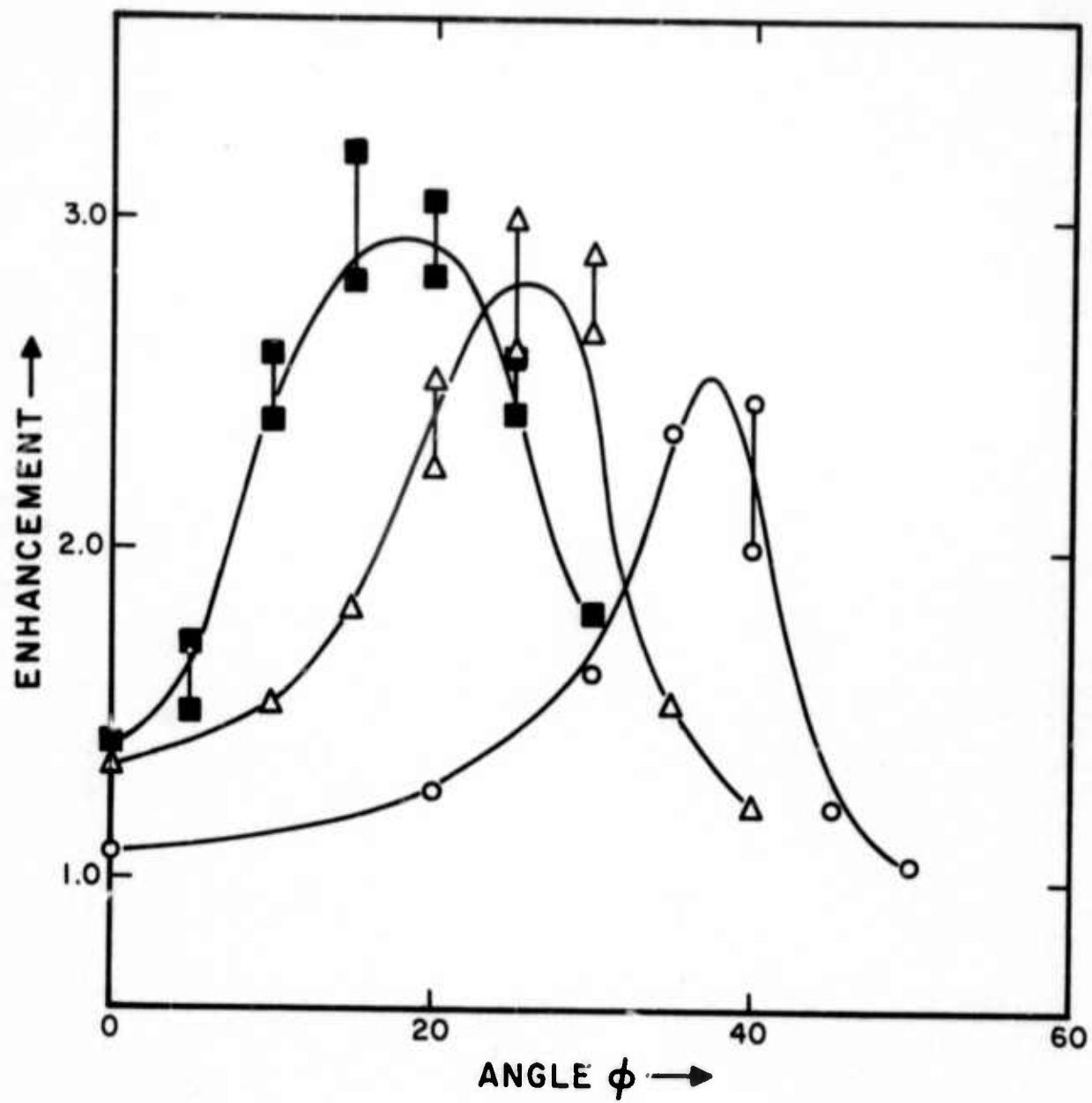


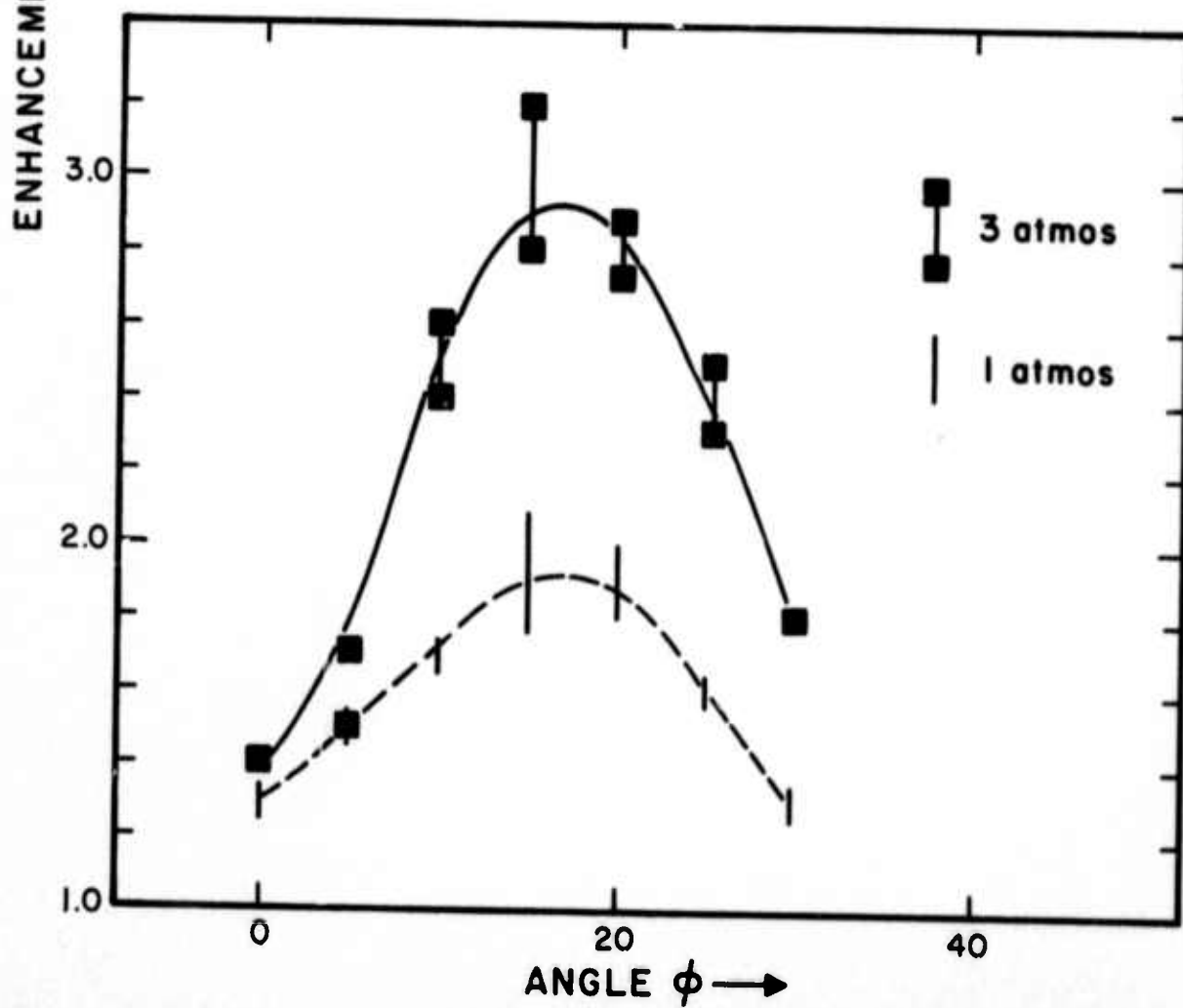
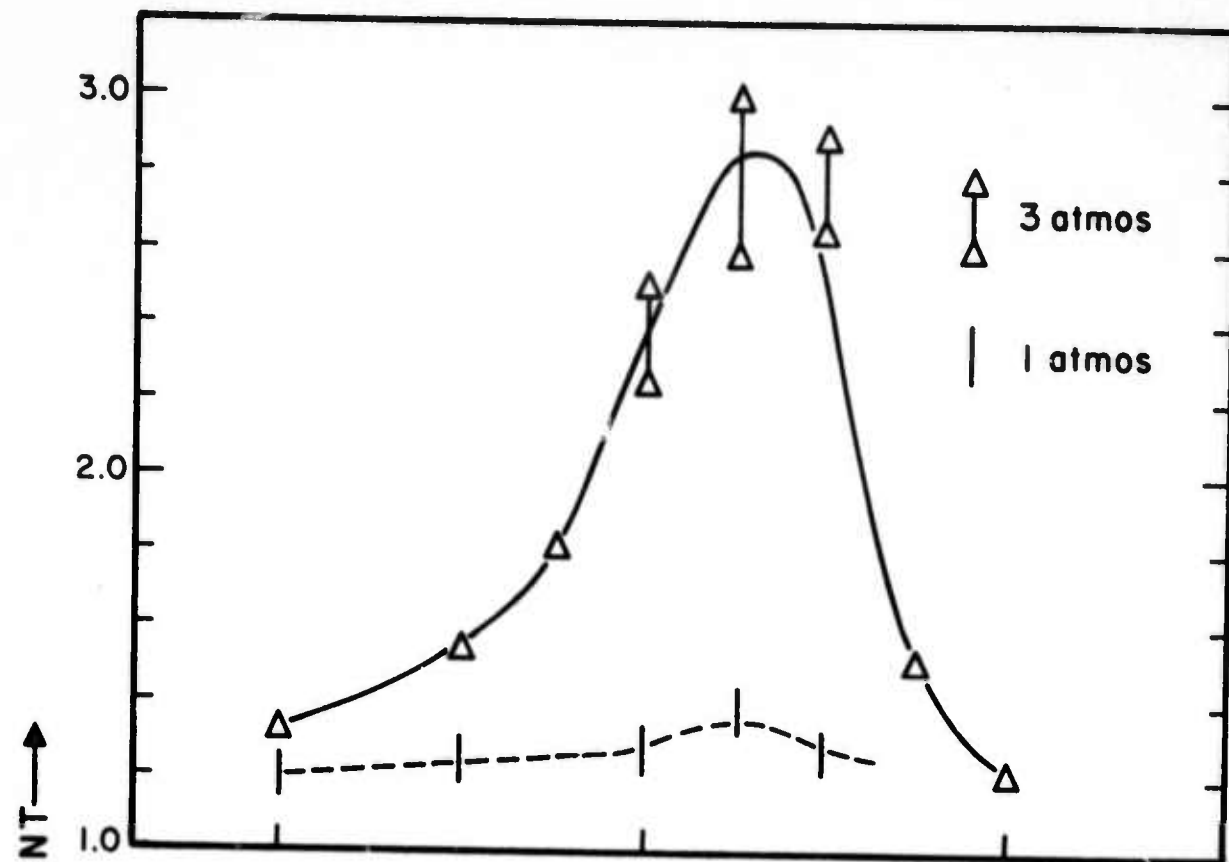
Figure 31 shows plots of the enhancement ratios for the 6400 \AA emission as functions of polarization angle ϕ for sampling plate inclinations of $1^{\circ}48'$ and $3^{\circ}36'$ to the Brewster angle at two pressures and 1 and 3 atmospheres. The ratio of excited state populations for the upper $3s^3\Sigma_u^+$ state is of the order of 30:1 for the three atmosphere data. Clearly seen is a substantial decrease in enhancement ratio comparable in order of magnitude to that expected for a decrease in gain per transit from the indicated 15% to approximately zero. (i.e. 1/30th). Such data is at least completely inconsistent with the converse hypothesis of a strongly absorptive transition for 6400\AA at 3 atmospheres. In the worst case it could indicate an unfortunate equality of population per state of upper and lower states at 3 atmospheres which is then shifted to a strongly absorptive ratio at 1 atmosphere, but such an interpretation seems unlikely in view of the large change of 30:1 in the ratio of the populations between the two pressures.

A more direct system for the measurement of gain or loss is under construction at the time of writing in which measurements of attenuation or enhancement will be achieved using a dye laser beam tuned to the resonant wavelength of the transition involved.

Figure 31

Cavity enhancement ratios for the 6400 \AA feature as functions of polarization angle ϕ for the two pressures in the HPAC-1b system, 1 and 3 atmospheres as indicated.

- a) Upper curve -, data obtained from sampling plate inclined $1^{\circ}48'$ to the Brewster angle.
- b) Lower curve - data obtained from sampling plate inclined $3^{\circ}36'$ to the Brewster angle.



V. IMPLICATIONS

The most evident implication of the technical results presented in the previous section is that had optical quality Brewster windows been used on HPAC-1b, it would have lased at 6400\AA at only 3 atmospheres pressure. It should again be emphasized that this is gain measured transversely to the e-beam over a relatively narrow column of afterglow. Such a result projects well to the planned higher-pressure cases in which the transverse dimension exceeds the range of the e-beam.

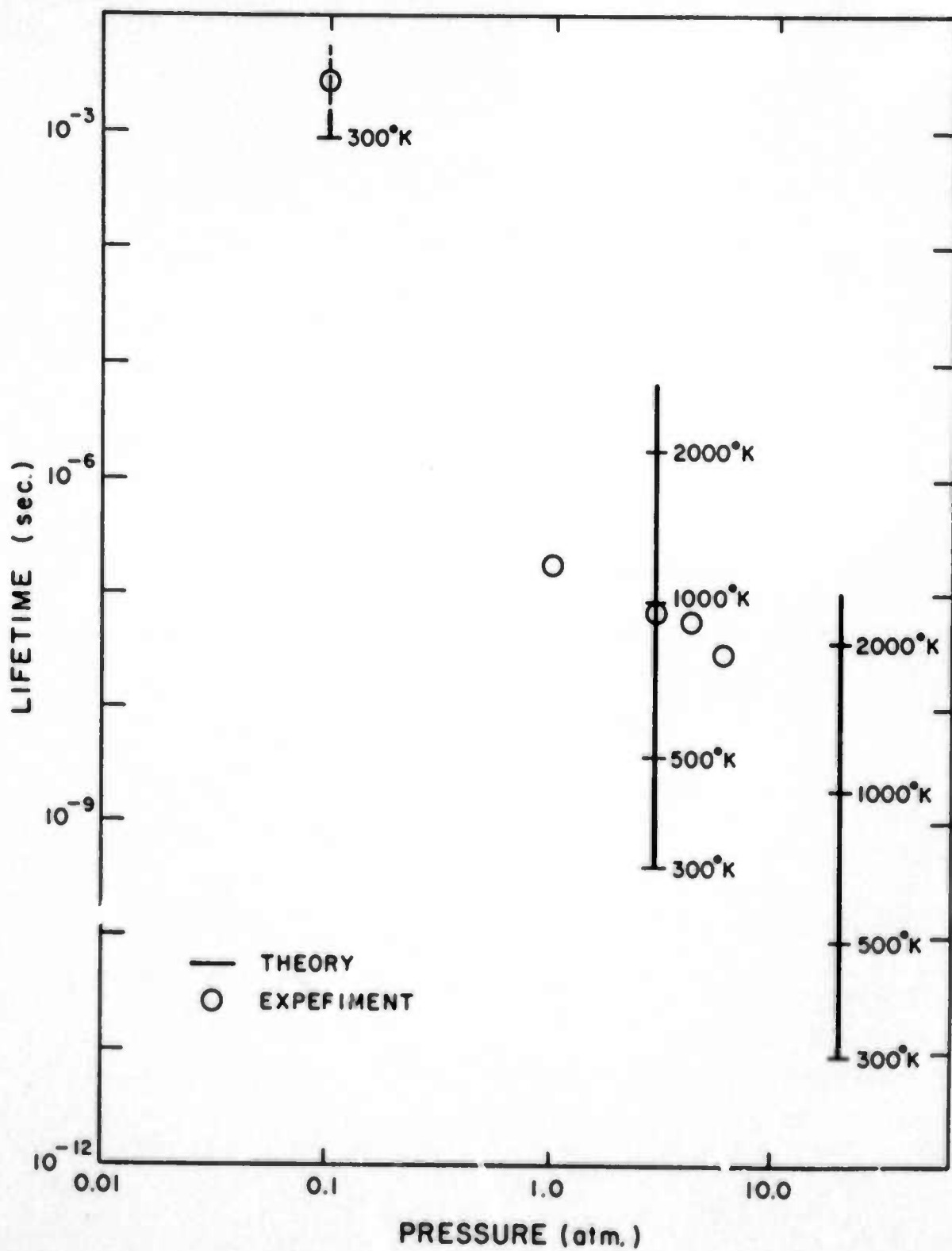
The more subtle implications are perhaps even more important. In particular:

- (1) The results summarized in Table III suggest that in helium collisional recombination does in fact offer a mechanism for optically recovering the majority of the excitation energy lost to ionization and wasted in analogous N_2 and H_2 e-beam laser systems.
- (2) The relatively short lifetimes summarized for the He_2 system in Table IV indicate that if these are in fact recombination lifetimes, as is indicated by the reciprocal plots such as Figures 22 through 24, then the possibility of unrealized higher order terms slowing the recombination has not yet become a problem at 4.2 atmospheres. This is of considerable significance, as is indicated in Figure 32, because now the range of parameters spanned by extrapolations to the objective lifetime of a nanosecond is small compared to the range over which measurements are available.

Neither the reheating of the electrons by the stabilizing processes nor an unexpected saturation of the sequence has become a problem. As can be seen, the experimental points on the 1 to 5 atmosphere interval are consistent with

Figure 32

Lifetimes as a function of pressure excited by the e-beam of the sources of population of states resulting from the collisionally-stabilized recombination of helium ions. Theory is shown by solid bars and experiment by open circles. Values are marked on the bars which correspond to the electron temperatures indicated.



theoretical calculations at an electron temperature of 1000°K. This temperature is in turn consistent with the extrapolations of the thermal economy calculations^{11,12} which predict the degree of temperature rise produced by the superelastic stabilizing collisions.

Clearly there is a much stronger basis for extrapolating the results of both experiments at 0.1 atmosphere and 3.0 atmospheres to a lifetime of a few nanoseconds at 20 atmospheres than there was initially on the basis of the first measurement alone. In fact, the recombination rate coefficient corresponding to the 75 nanosecond lifetime and electron density $[e] = 5 \times 10^{14} \text{ cm}^{-3}$ is

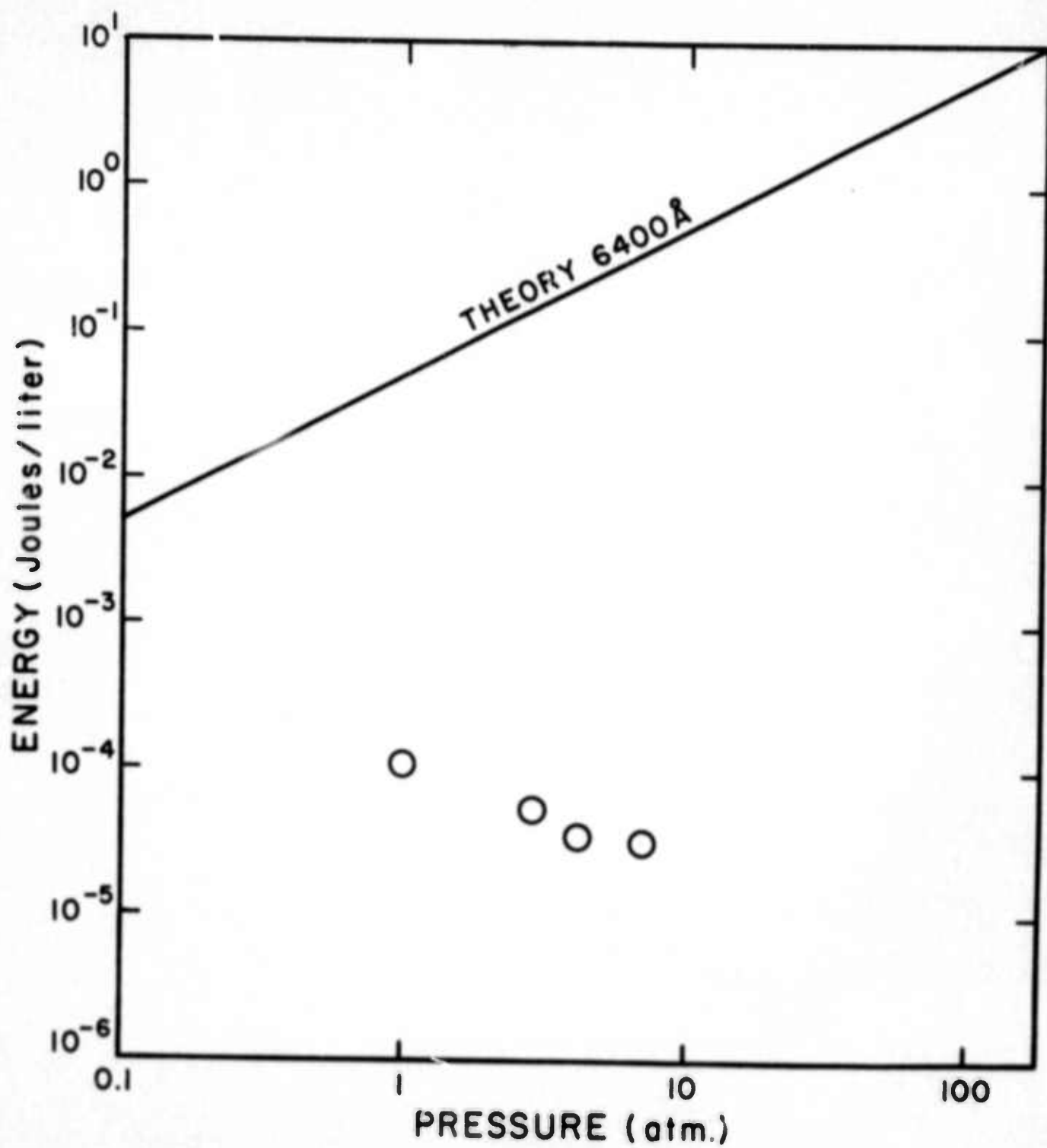
$$\alpha = 2.7 \times 10^{-8} \text{ cm}^3 \text{ sec}^{-1}, \quad (23)$$

and represents one of the largest values measured for collisional recombination in the absence of dissociative recombination. It is confirming evidence that the parameterizations such as (4) can indeed be considered valid to such large values.

- (3) The implication of the rather low efficiencies for the incoherent emission of radiation from the recombination as shown in Table V is that much of the stabilization is carried by non-radiative collisional channels. However, in this case, the prospect for reducing the importance of such channels by the competition from a lasing channel is good in view of the high preliminary values of gain. Figure 33 presents the comparison of experiment and theory as a guide to potential extrapolation of energy available in the 6400Å band. The present experiment is about three orders of magnitude below the energy corresponding to the quantum efficiency of the

Figure 33

Energy/liter per pulse as a function of gas pressure calculated to be available to the 6400Å transition in He_2 in the afterglow of the recombining e-beam discharge. The experimental points reported in this paper are shown by the open circles.



transition. The improvement introduced by lasing is a very important parameter to obtain.

- (4) Finally it should be re-emphasized that the gain inferred in the 6400Å transition indicates that the system should lase in an afterglow container having high-quality Brewster-angle windows and the same excitation conditions. The difficulty in constructing high-pressure, UHV-quality, laser-quality Brewster-angle windows had prevented their implementation on HPAC-1, and 1b. However, the windows have now been fabricated and are scheduled to be installed with HPAC-3 which will allow operation to 20 atmospheres. Then the critical test of the gain measurements can be performed.

References

1. D. R. Bates, A. E. Kingston, and R. W. P. McWhirter, Proc. Roy. Soc. (London) A267, 297 (1962).
2. D. R. Bates and S. P. Khare, Proc. Phys. Soc. (London) 85, 231 (1965).
3. C. B. Collins, Phys. Rev. 177, 254 (1969).
4. C. B. Collins, Phys. Rev. 186, 113 (1969).
5. D. R. Bates and A. E. Kingston, Planet. Space Sci. 11, 1 (1963).
6. C. B. Collins, unpublished report.
7. J. Berlande, M. Cheret, R. Deloche, A. Gonfalone, and C. Manus, Phys. Rev. A1, 887 (1970).
8. E. Hinnov and J. G. Hirschberg, Phys. Rev. 125, 795 (1962).
9. C. B. Collins, H. S. Hicks, W. E. Wells, and R. Burton, Phys. Rev. 6, 1545 (1972).
10. C. B. Collins, H. S. Hicks, and W. E. Wells, Phys. Rev. A2, 797 (1970).
11. D. R. Bates and A. E. Kingston, Proc. Roy. Soc. A279, 10 (1964).
12. D. R. Bates and A. E. Kingston, Proc. Roy. Soc. A279, 32 (1964).
13. C. B. Collins, Recombination Laser, Report No. UTDPA A002-1, ONR Contract No. N00014-67-A-0310-0007, 1972.
14. C. B. Collins and W. W. Robertson, J. Chem. Phys. 40, 701 (1964).
15. L. Blamaru, J. Appl. Phys. (Publication pending)
16. R. Ladenburg and F. Reiche, Ann. Physik, 42, 181 (1913).